© 2019. Published by The Company of Biologists Ltd | Journal of Cell Science (2019) 132, jcs222083. doi:10.1242/jcs.222083

RESEARCH ARTICLE

GM130 and p115 play a key role in the organisation of the early secretory pathway during skeletal muscle differentiation

Emiliana Giacomello[1,2,*], Paolo Ronchi[3] and Rainer Pepperkok[1,*]

ABSTRACT

Skeletal muscle (SKM) differentiation is a highly regulated process leading to the formation of specialised cells with reorganised compartments and organelles, such as those of the early secretory pathway. During SKM differentiation the Golgi complex (GC) redistributes close to the nuclear envelope and in small distinct peripheral structures distributed throughout the myotube. Concurrently, GC elements closely associate with endoplasmic reticulum-exit sites (ERES). The mechanisms underlying this reorganisation and its relevance for SKM differentiation are poorly understood. Here, we show, by time-lapse imaging studies, that the changes in GC organisation involve GC fragmentation and redistribution of ERES with the formation of tightly associated GC–ERES units. We show that knockdown of GM130 (also known as GOLGA2) or p115 (also known as USO1), two regulators of the early secretory pathway, impairs GC and ERES reorganisation. This in turn results in inhibition of myotube fusion and M-cadherin (also known as CDH15) transport to the sarcolemma. Taken together, our data suggest that the correct reorganisation of the early secretory pathway components plays an important role in SKM differentiation and, thus, associated pathologies.

KEY WORDS: Golgi compartment, ER-exit site, Skeletal muscle differentiation, M-cadherin

INTRODUCTION

Myogenesis is a complex and highly regulated process that results in the formation of multinucleated cells named myotubes (Braun and Gautel, 2011; Buckingham and Rigby, 2014), which further differentiate in mature skeletal muscle (SKM) cells called myofibres. After the initiation of the myogenic differentiation programme (Braun and Gautel, 2011; Buckingham and Rigby, 2014), the subsequent phases of myogenesis are characterised by cell fusion accompanied by the reorganisation of pre-existing compartments and organelles (Franzini-Armstrong, 2004; Ralston, 1993), including vesicular trafficking components (Kaisto and Metsikko, 2003; Rossi et al., 2008; Volpe et al., 1992).

The formation of multinucleated myotubes is a multistep process entailing initial recognition and adhesion between myoblasts, their alignment, and finally membrane breakdown and fusion (Doberstein et al., 1997). This process requires the interplay of several factors, among them the protein M-cadherin (also known as CDH15) has been proposed to exert a pivotal role by mediating cell–cell adhesion (Donalies et al., 1991). M-cadherin is member of the cadherin family, a group of transmembrane glycoproteins, that mediate Ca^{2+}-dependent homophilic cell–cell adhesion and play a crucial role during SKM differentiation (Donalies et al., 1991). M-cadherin expression is upregulated in SKM cell lines during myotube formation, and declines after completion of this process. Conversely, M-cadherin inhibition impairs myoblast fusion (Pouliot et al., 1994; Zeschnigk et al., 1995).

In most eukaryotic cells, three main endoplasmic reticulum (ER) subcompartments can easily be recognised: rough ER, smooth ER and ER-exit sites (ERES). However, in adult SKM cells the distinction of the three subcompartments is more complicated. During early SKM cell differentiation smooth ER undergoes a series of modifications that lead to the formation of the sarcoplasmic reticulum (SR), responsible for Ca^{2+} homeostasis and present in close association with transverse tubules for muscle contraction (Rossi et al., 2008). Interestingly, in this process, the early secretory pathway components also change their distribution. The Golgi complex (GC) undergoes architectural modifications that result in the formation of a perinuclear rim and dispersed elements along the myotube (Kaisto and Metsikko, 2003; Rossi et al., 2008; Volpe et al., 1992). Later, in muscle fibres, the GC perinuclear rim is lost and the GC appears as very small elements, localised nearby the nucleus and in the fibre body in a fibre-type dependent manner (Ralston et al., 1999). These GC elements are very small compared to other cell types; however, each element maintains the typical stacked organisation (Ralston et al., 1999). The GC reorganisation coincides with the remodelling of the microtubule network and changes of the microtubule-organising centre from being a classic centrosome into a combination of a perinuclear belt and centrosomal remnants in the cell body (Tassin et al., 1985a, b; Zaal et al., 2011). Interestingly, GC reorganisation involves also its close localisation with ERES that, in differentiating muscle cells, progressively cluster in proximity of the GC (Ralston et al., 1999; Lu et al., 2001). The organisation of GC in peripheral small elements has been suggested to occur because a relocation of the ERES near to the microtubule minus end induces the *de novo* assembly of a GC structure at this location (Lu et al., 2001). However, more recently it has been hypothesised that GC reorganisation could entail more complex mechanisms, such as the progressive modification of existing structures (Zaal et al., 2011). The mechanism underlying this transition, and the influence of such unique morphology on SKM differentiation, has not yet been elucidated.

The growing opinion that GC and ERES are capable of a reciprocal fine regulation (Glick, 2014; Ronchi et al., 2014), and the increasing evidence of a strong correlation between human diseases and the shape and function of the GC (Bexiga and Simpson, 2013; Percival and Froehner, 2007) oriented our work at further understanding the mechanisms responsible of the close

[1]Cell Biology and Biophysics Unit, European Molecular Biology Laboratory, (EMBL), Meyerhofstraße 1, Heidelberg D-69117, Germany. [2]Department of Medicine, Surgery and Health Sciences, University of Trieste, Trieste 34149, Italy. [3]Electron Microscopy Core Facility, Europen Molecular Biology Laboratory (EMBL), Meyerhofstraße 1, Heidelberg D-69117, Germany.

*Authors for correspondence (egiacomello@units.it; pepperko@embl.de)

E.G., 0000-0003-3329-6269; R.P., 0000-0002-9762-3583

Received 2 July 2018; Accepted 20 December 2018

Journal of Cell Science (2019) 132, jcs222083. doi:10.1242/jcs.222083

correlation between GC and ERES and its importance for SKM differentiation and fusion.

Our results show that the changes in GC organisation in differentiating SKM cells involve GC fragmentation and redistribution of ERES with the formation of GC–ERES units. Knockdown experiments showed that GM130 (also known as GOLGA2) and p115 (also known as USO1) are involved in GC and ERES localisation in differentiating cells, and can inhibit myotube fusion by interfering with M-cadherin transport to the plasma membrane. Taken together, our data suggest that the correct reorganisation of the early secretory pathway components plays an important role in SKM differentiation.

RESULTS

In myotubes, the GC and ERES form dynamic units by redistributing predominantly pre-existing GC membranes

Aiming to further elucidate the mechanisms underlying the reorganisation of GC peripheral structures in differentiating SKM cells, and to understand to what extent they form *de novo* or from pre-existing membranes, we analysed GC and ERES distribution in differentiating C_2C_{12} cells by immunostaining and live-cell imaging. As previously reported, C_2C_{12} cells undergo differentiation upon medium exchange, giving rise to a cell population with different degrees of differentiation, where the GC and ERES reorganise into a specific pattern (Lu et al., 2001). We first analysed the reciprocal localisation of ERES and GC in cells exposed for different times to differentiation medium by quantifying the colocalisation levels of Sec13 and GM130, markers for ERES and GC respectively (Fig. 1A–C). The mean Pearson coefficient of the Sec13 and GM130 labelling, which was used as measure for colocalisation, increased with the time when the cells were exposed to differentiation medium (Fig. 1B) confirming that ERES and GC become intimately associated during muscle differentiation. Consistent with this, by analysing the relative frequency of the Pearson coefficient, we could observe a shift of the cell population towards higher Pearson coefficients after 24 and even more after 48 h of exposure to differentiation medium, compared to undifferentiated cells (Fig. 1C). We qualitatively scored GC shape modifications and changes in ERES localisation during differentiation (Fig. 1A). We subdivided undifferentiated and differentiating cells in four distinct phases based on their GC and ERES distribution. In phase 0, where cells have not yet started to differentiate based on the absence of the differentiation marker α-actinin, the GC forms a ribbon located at one side of the nucleus (Fig. 1A, undifferentiated cells are marked with a white circle). In phase 1, cells start to express visibly α-actinin and to redistribute the GC around the nucleus (Fig. 1A, phase 1 cells are marked with a white square, arrowheads point towards the perinuclear rim). In both phase 0 and phase 1, ERES localise throughout the cell as discrete structures, the majority of which are not localised near to GC structures as highlighted in the line scans in Fig. 1A (Sec13 profile in green and GM130 in red). In phase 2 (Fig. 1A, cells marked with an asterisk), cells show a more complete redistribution of the GC around the nuclear envelope (Fig. 1A, arrowheads) and some emerging peripheral structures (Fig. 1A, double arrowheads point towards the peripheral structures). At the same time ERES concentrate close to the GC, and the number of structures diffused in the rest of the cell appears reduced as shown by the line scan of the fluorescent signal of the GC and ERES. In phase 3 cells form elongated myotubes (Fig. 1A, cell with double asterisk) with several GC peripheral elements throughout the cell (Fig. 1A, cell with double asterisk, see double arrowheads) and ERES are predominantly localised close to these GC structures.

During SKM differentiation, the ER undergoes a series of modifications such as the expression of muscle-specific SR proteins and the formation of specialised domains (Ralston, 1993; Rossi et al., 2008). Consistent with data previously reported, the detection of the ER marker protein disulfide-isomerase (PDI, also known as P4HB) in Fig. 1D further shows that the transformation from undifferentiated myoblasts to differentiated myotubes involves the transition from a reticular dense ER to a thinner ER, which is distributed throughout the entire cell, mainly aligned along the myotube axis (Ralston, 1993)

Live-cell imaging of differentiating cells transfected with the GC marker Golgi–CFP and the ERES marker Sec23a–EYFP allowed us to monitor the dynamics of ERES and GC over time (Fig. S1). GC and ERES fluorescence signals were segmented, and the ratio between ERES fluorescence in the GC and the total ERES fluorescence were analysed over time. Quantifying the ERES fluorescence and superimposing with the GC fluorescence value showed that this value remained almost constant over time in phase 0 cells (Fig. S1, cell A). In contrast, in a cell passing from phase 0 to 2 (Fig. S1, cell B) the proximity of the two markers increased steadily, approaching a plateau level within 5 h. Cells in phase 3 (Fig. S1, cell C) steadily maintain the plateau level.

The transition from phase 1 to phase 2 was characterised by the formation of several new peripheral GC structures. To address the question as to what extent these GC peripheral structures form *de novo* or from pre-existing GC membranes, we imaged phase 1–2 differentiating C_2C_{12} cells for 15 min at 10 s time intervals (Fig. 2A–D; Movies 1–4). The analysis revealed a variety of events (Fig. 2A–E). We observed 2.4±1.2 GC splitting events per cell, where a GC element detaches from the pre-existing GC (Fig. 2A,B,E). Fig. 2A,B and Movies 1 and 2 show such an event with a peripheral GC element forming by detaching from the perinuclear region (Fig. 2A), or the splitting of a GC element into two separated elements (Fig. 2B). In addition 1.6±0.9 merging events per cell, consisting of the fusion of two already separated GC structures, were also observed (Fig. 2B,E). Only rarely (0.25 events/cell) did new GC elements appear without any relation to pre-existing GC structures, which is possibly attributable to *de novo* biogenesis of these GC structures (Fig. 2D,E). Taken together, these data support the hypothesis that the changes in GC distribution during the early phases of SKM differentiation predominantly involve the reorganisation of pre-existing GC elements. Interestingly, most GC elements observed were accompanied by a group of ERES close by (arrowheads in Fig. 2A,B and Movies 1 and 2 point towards a Golgi structure surrounded by ERES) that displaced in a syntonic fashion, indicating that these two entities move as a unit once it has formed (see arrowheads in Fig. 2A–D and Movies 1–4).

The data described above, together with previous work showing that GC and ERES organisation persist despite the lack of normal microtubule tracks in differentiating SKM cells (Zaal et al., 2011), and the growing evidence of a reciprocal regulation of GC and ERES (Glick, 2014; Ronchi et al., 2014), introduces the hypothesis that the GC also has a leading role in ERES positioning in differentiating C_2C_{12} cells. To test this hypothesis, we perturbed the GC organisation by treating cells with the fungal metabolite brefeldin A (BFA) (Lippincott-Schwartz et al., 1989) and followed ERES behaviour in differentiating SKM cells. As shown in Fig. 3A,B and Movie 5, BFA treatment of phase 2 or 3 C_2C_{12} cells resulted in the disappearance of GC structures. Most of the perinuclear GC

Journal of Cell Science (2019) 132, jcs222083. doi:10.1242/jcs.222083

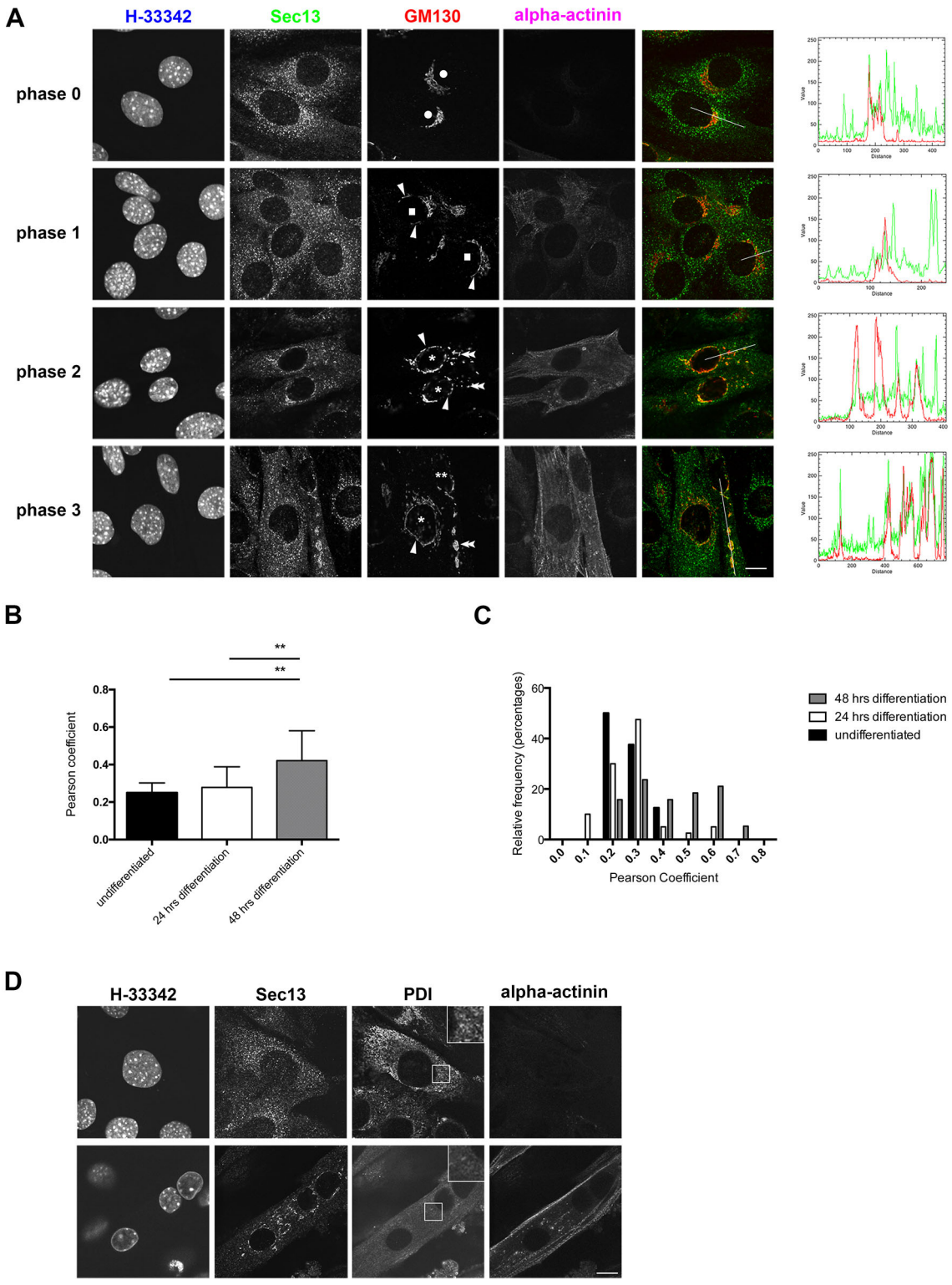

Fig. 1. Reciprocal localisation of GC and ERES during SKM differentiation. Undifferentiated, and C_2C_{12} cells that had been induced to differentiate for 24 h and 48 h were fixed and immunostained for the GC marker GM130, the ERES marker Sec13 and α-actinin, as an SKM differentiation marker. Hoechst 33342 was used to stain nuclei. (A) Undifferentiated and differentiated cells stained with anti-GM130 and -Sec13 antibodies. In the merged image only Sec13 (green) and GM130 (in red) are shown. Undifferentiated cells are marked with a white circle, phase 1 cells are marked with a white square, phase 2 cells are marked with an asterisk, and a phase 3 myotube is indicated with two asterisks; arrowheads highlight the perinuclear region, double arrowheads point to GC peripheral structures. In each merged image, a line from the centre of the nucleus to the periphery has been drawn and the relative plot profile is reported for each phase. (B) The colocalisation of GM130 and Sec13 expressed as the Pearson coefficient, in undifferentiated, and 24 h and 48 h differentiated C_2C_{12} cells. (C) Data are expressed as the distribution of Pearson coefficients in undifferentiated and 24 or 48 h differentiated cells (n=85; $^{**}P$<0.01). Data are expressed as means±s.d. (D) Cells were immunostained for the ER marker PDI, the ERES marker Sec13 and α-actinin. The magnified insets capture the reticular dense ER in undifferentiated and the thinner ER in differentiated cells, respectively. Scale bar: 10 µm.

Journal of Cell Science (2019) 132, jcs222083. doi:10.1242/jcs.222083

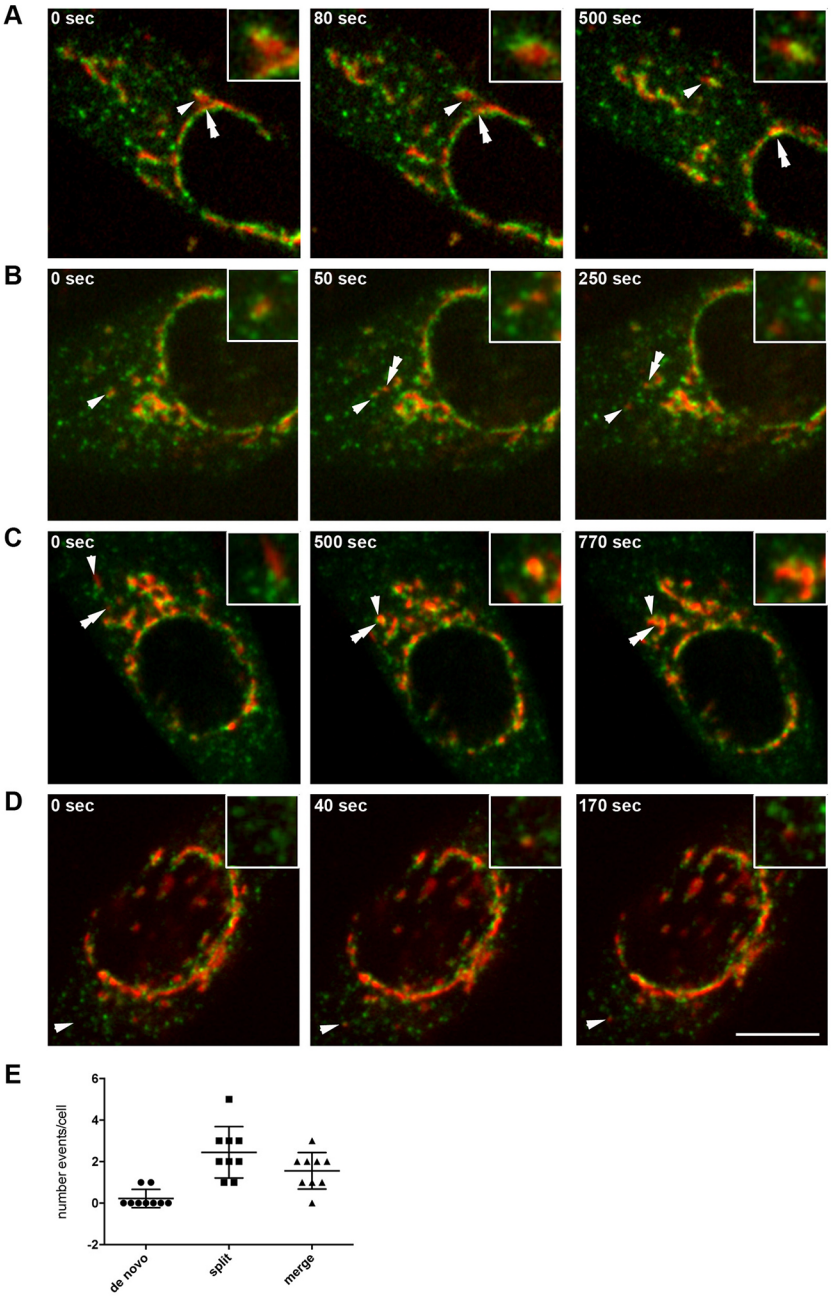

Fig. 2. Reorganisation of GC and ERES during SKM differentiation. (A–D) C_2C_{12} were transfected with Golgi–CFP (red) and Sec23a–EYFP (green), induced to differentiate, and imaged every 10 s in the multi-position time-lapse spinning disc confocal microscope. *Z*-stacks covering the entire cell were acquired and sum projections are reported. Selected still images of GC and ERES reciprocal positioning in differentiating C_2C_{12} cells are reported for GC splitting (A,B), GC merging (C) and GC *de novo* biogenesis (D) (see corresponding Movies 1–4). In A, the arrowhead points towards a Golgi element that detaches from the perinuclear GC (double arrowhead) and moves to the cell periphery. In B, the arrowhead and double arrowheads point towards a peripheral Golgi element that splits into two elements that move in different directions during the acquisition. In C, the arrowhead and the double arrowhead point towards two distinct Golgi elements that move in the cell, change shape and meet to merge. In D, indicated by the arrowhead, the appearance of a GC structure consistent with its *de novo* synthesis is shown. Scale bar: 10 µm. The magnified insets capture the GC structures and surrounding ERES as indicated by the arrowheads and double arrowheads. (E) Graph reporting the mean splitting, merging or *de novo* biogenesis events observed per cell (n=9). Means±s.d. are also reported.

structures close to the nuclear envelope (Fig. 3A, see arrows and fluorescence line scans) and most peripheral GC elements disappeared, indicative of the well-described re-absorption of GC enzymes to the ER after BFA treatment (Lippincott-Schwartz et al., 1989). Coincident with this, the perinuclear localisation of ERES changed significantly (Fig. 3A, fluorescence line scans), while bigger fluorescent dots appeared in the perinuclear region and throughout the cell (see arrowheads in Fig. 3A,B). These bigger Sec23a–YFP-positive structures showed a close proximity with the immunofluorescence signal for the GC matrix protein GM130 (Fig. 3B, see arrowheads and fluorescence line scan).

GM130 and p115 are required for the formation of ERES–GC units during C_2C_{12} cell differentiation

The evidence described above and previous data showing that GM130 is involved in a membrane-tethering mechanism (Nakamura et al., 2010; Seemann et al., 2000) raised the question of whether GM130 could play a role in the organisation of GC–ERES units during SKM differentiation. Based on previous data from the literature demonstrating a direct interaction between GM130, p115 (Nakamura et al., 1997) and GRASP65 (also known as GORASP1) (Barr et al., 1998; Barr et al., 1997), we transfected C_2C_{12} cells with siRNAs targeting the three proteins and analysed the effects on GC and ERES distribution both in undifferentiated and differentiated cells. In undifferentiated C_2C_{12} cells, knockdown of GM130, p115 or GRASP65 resulted in no apparent changes in Golgi morphology (Fig. 4A). However, we observed that the number of ERES in proximity of the GC was reduced upon single knockdown of all the three proteins (Fig. S2C). In parallel, electron microscopy (EM) analyses showed minor differences in the ultrastructure of the GC upon depletion of the different proteins (Fig. S2A). With all treatments, the GC appeared stacked and the

Journal of Cell Science

Journal of Cell Science (2019) 132, jcs222083. doi:10.1242/jcs.222083

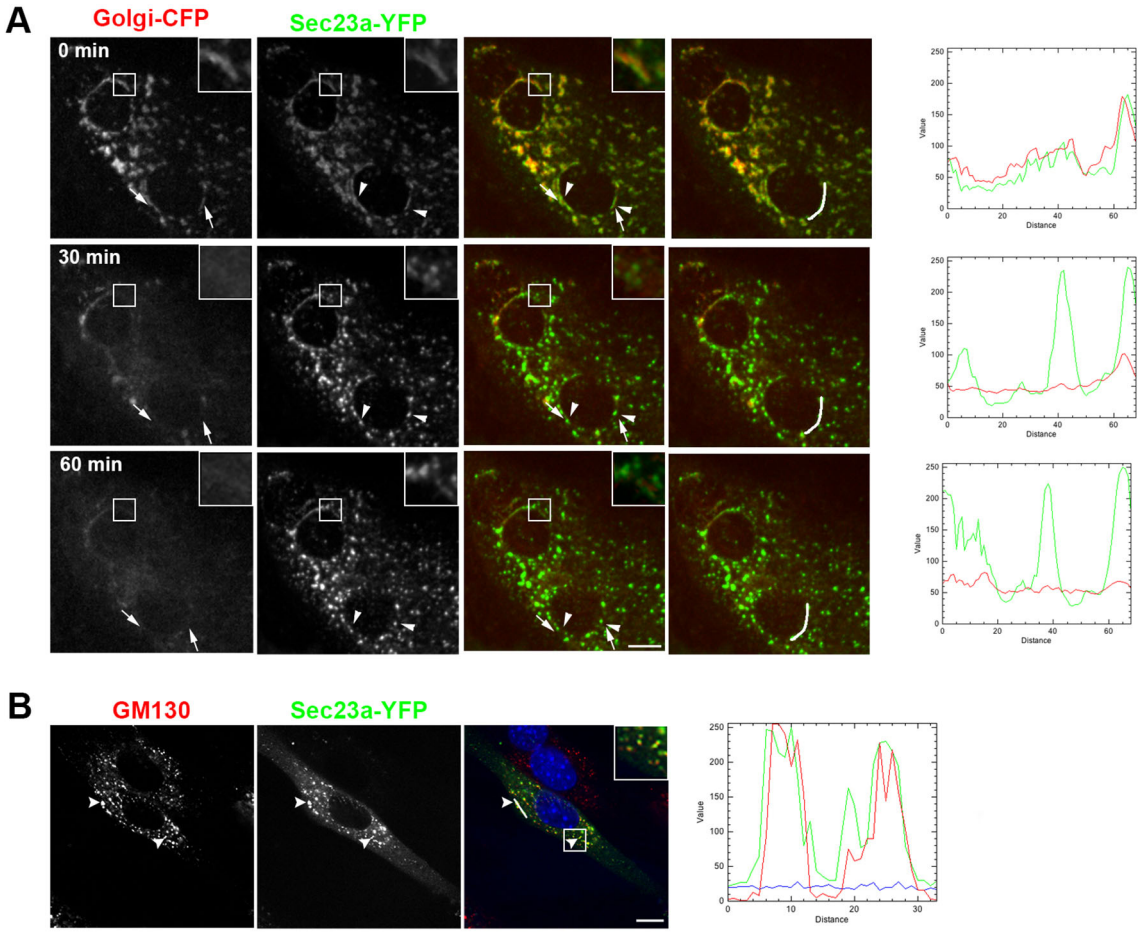

Fig. 3. Effects of BFA treatment in differentiating C_2C_{12} cells. C_2C_{12} cells were transfected with Golgi–CFP (red) and Sec23a–EYFP (green), induced to differentiation and treated with BFA. (A) Images of selected time-points from BFA-treated cells imaged in the multi-position time-lapse spinning disc confocal microscope every 5 min. *Z*-stacks covering the entire cell were acquired and sum projections are reported (see also Movie 5). The treatment of differentiating myotubes with BFA induces the gradual disappearance of the characteristic perinuclear GC structures (arrows and inset) resulting in almost complete loss of the CFP signal after 60 min. The typical perinuclear Sec23a–EYFP signal is lost and accumulates in small dots (see arrowheads). In each merged image, from the three reported time-points, a 4-pixel wide line around the perinuclear region has been drawn and the relative plot profile is reported for each phase. (B) Images of BFA-treated cells stained with an anti-GM130 antibody (red), showing that the Sec23a–EYFP (green) signal concentrates in the proximity of GM130 (red)-positive structures as highlighted by the arrowheads and by the relative fluorescence plot profile. Hoechst 33342 was used to stain nuclei. Scale bars: 10 µm.

morphology was consistent with the observed GC structure in control cells. Quantitative analysis of the number of ERES surrounding the GC, measured by counting the number of ERES and normalising for the length of the ER sheets within ∼1 µm of the surface of the nearest GC, showed a reduction for all siRNAs (Fig. S2B), consistent with the immunofluorescence data (Fig. S2C). However, as previously reported for GM130 (Tangemo et al., 2011), none of the siRNA treatments showed an effect on ER to plasma membrane transport of the well-established transport marker, the viral protein VSVG as shown in Fig. 4B, suggesting that, in undifferentiated cells, knockdown of these proteins and the resulting morphological changes in ERES are not playing a major role for VSVG traffic.

When cells were exposed to differentiation medium, differentiating C_2C_{12} cells started to express the muscle differentiation markers α-actinin, M-cadherin and junctophilin 2 (JP2, also known as JPH2) similar to cells treated with the negative control (Neg9) siRNA (Fig. 4D,E; see also Fig. S3).

Interestingly, once induced to differentiate, C_2C_{12} cells treated with GM130 and p115 siRNAs showed profound effects in the organisation of the early secretory pathway components compared to control and GRASP65-depleted cells (Fig. 5A–D). In GM130-knockdown cells, the distribution of GC structures was clearly different from control cells (Fig. 5A). The GC appeared more compact with fewer peripheral elements and did not surround the perinuclear region. Quantification showed that the percentage of nuclei with perinuclear GC staining was significantly reduced from 46.8±3.5% in Neg9 siRNA treated cells to 24.4±5.4% in GM130 knockdown cells (mean±s.d.; graph in Fig. 5B). Interestingly, upon staining with the ERES-specific antibody anti-Sec13, we could observe that, in GM130-knockdown C_2C_{12} cells, ERES were rarely concentrated at the perinuclear region or clustered in peripheral elements as occurs in Neg9-transfected cells (Fig. 5D), but rather were present throughout the cell. Depletion of p115 resulted in a phenotype very similar to the one observed in GM130-knockdown cells (see Fig. 5A–D). Colocalisation analyses with the nucleoporin p62 (also known as NUP62) (Fig. S4A), which localises at the nuclear envelope, revealed that GM130 and p115 depletion prevents the accumulation of ERES at the perinuclear rim (Fig. 5C, Fig. S4A). On the contrary, GRASP65 depletion did not cause major changes in GC or ERES distribution compared to control cells (Fig. 5A–D; Fig. S4A).

Journal of Cell Science (2019) 132, jcs222083. doi:10.1242/jcs.222083

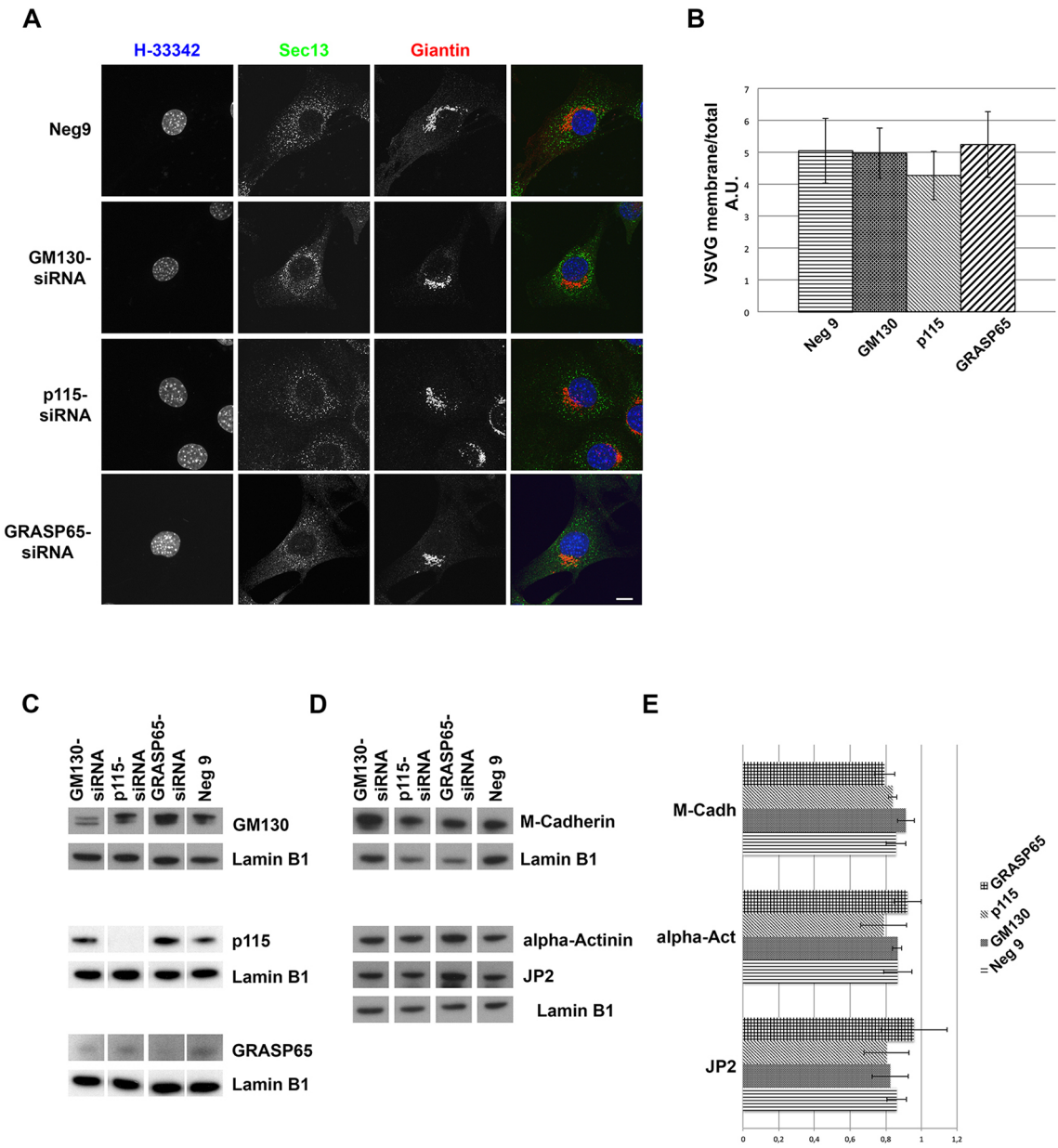

Fig. 4. Analysis of the effects of Golgi compartment proteins knockdown in undifferentiated C_2C_{12} cells. Cells were transfected with Neg9, GM130, p115 and GRASP65 siRNAs, and, after 48 h, subjected to different analyses. (A) Cells were stained with anti-giantin and -Sec13 antibodies, and Hoechst 33342 to stain nuclei. Scale bar: 10 µm. (B) Graph reporting the efficiency of VSVG transport to the membrane. (C–E) Protein expression analyses of selected skeletal muscle proteins upon siRNA transfection. Cells were transfected with siRNAs, and after 48 h, induced to differentiate for 48 h, and then collected for western blot analyses. (C) Protein expression levels of GM130, p115, and GRASP65 upon siRNA inhibition. (D) Protein expression levels of the SKM markers α-actinin, junctophillin 2 (JP2) and M-cadherin. Protein loading was normalised with Lamin B1. (E) Quantification of the protein expression levels. Data reported are the mean±s.d. of three independent experiments.

In order to understand whether the loss of clustering of ERES was specific or involved other vesicular systems, as COPI vesicles, we stained GM130- and p115-knockdown cells with EAGE antibody (Pepperkok et al., 1993). Interestingly, in contrast to what was observed for the distribution of ERES, both in GM130- and p115-knockdown cells, the vesicular protein complex COPI was accumulating in close proximity to GC structures (see Fig. S5) as in control cells.

As further support of our observations, we analysed GC and ERES morphology and distribution upon GM130, p115 and GRASP65 knockdown by means of electron microscopy. Consistent with the immunofluorescence analysis (Fig. 1A), electron tomography of the perinuclear region revealed morphological differences of the early secretory pathway between undifferentiated and differentiated C_2C_{12} cells (Fig. 6A). In undifferentiated myoblasts, the perinuclear ER regions are normally flat (in Fig. 6A, left panel), while the perinuclear ER in differentiated cells is rough (Fig. 6A, right panel) with several invaginations facing the nearby GC structures (Fig. 6A, right panel, black arrows), which are attributable to ERES as previously demonstrated by Lu and co-workers (Lu et al., 2001). Indeed, when observed on thin sections, the evaginations or buddings of the perinuclear ER pointing towards the GC, are decorated with an electron-dense coat that can be ascribed to the COPII coat (see Fig. 6B, Neg9, black arrow) (Lu et al., 2001).

Journal of Cell Science

Journal of Cell Science (2019) 132, jcs222083. doi:10.1242/jcs.222083

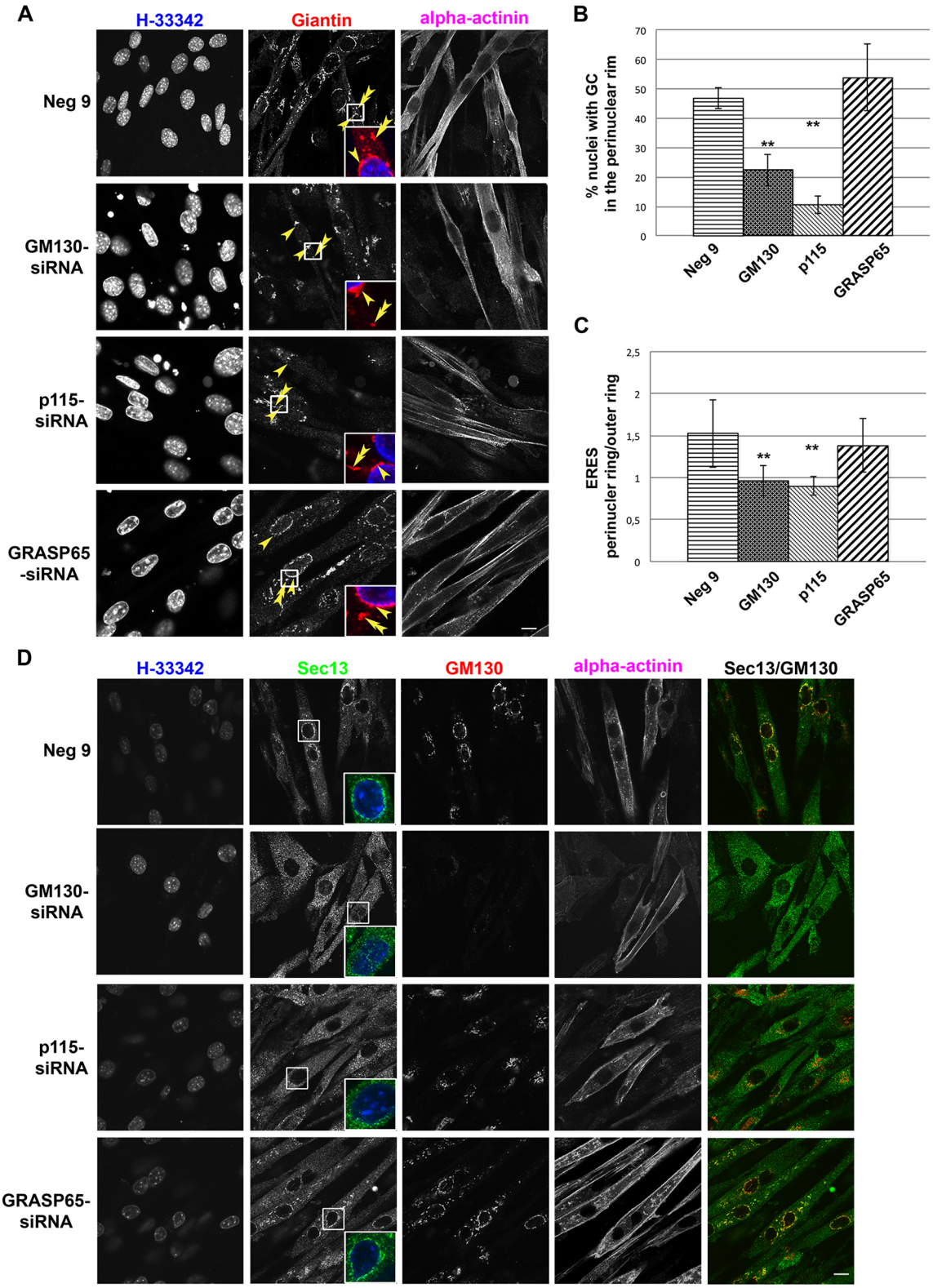

Fig. 5. Characterisation of the effects of GM130, p115 and GRASP65 knockdown on the GC and ERES distribution in differentiating C_2C_{12} cells. Cells were transfected with described siRNAs, and, after 48 h, induced to differentiate for 48 h, before being fixed and stained with the GC and ERES markers. (A) siRNA-transfected cells were stained with an anti-giantin polyclonal antibody to detect GC morphology, and anti-α-actinin antibody as a marker of differentiating SKM cells, and Hoechst 33342 to stain nuclei. Arrowheads highlight the perinuclear area and double arrowheads point towards the GC peripheral elements. The magnified insets capture the perinuclear distribution of GC. (B) Percentage of myotubes with perinuclear Golgi as detected by staining with anti-giantin antibody (data reported are the mean of three independent experiments; $^{**}P<0.01$). (C) Perinuclear localisation of Sec13 ($n=168$ from two independent experiments; $^{**}P<0.01$; see also Fig. S4A,B). Data are expressed as means±s.d. (D) Differentiating myotubes were stained with anti-GM130 and -Sec13 antibodies, and α-actinin was used to detect differentiating SKM cells, and Hoechst 33342 to stain nuclei. The magnified insets capture the perinuclear region to highlight ERES distribution at this site in different conditions. Scale bar: 10 µm.

Journal of Cell Science

Journal of Cell Science (2019) 132, jcs222083. doi:10.1242/jcs.222083

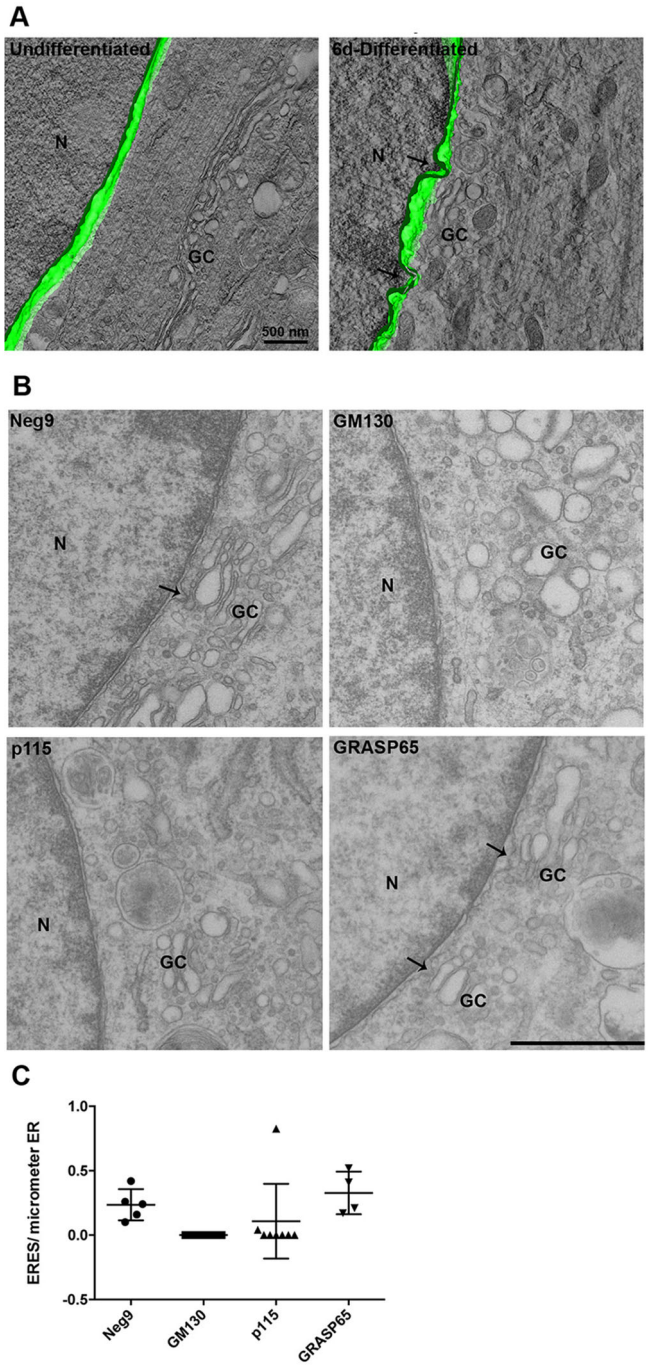

Fig. 6. Ultrastructural analysis of the perinuclear ER in undifferentiated, differentiated and knockdown C_2C_{12} cells. (A) An electron microscopy tomography reconstruction of the perinuclear ER (N, nucleus; GC, Golgi compartment; the perinuclear ER is reconstructed in green) of an undifferentiated cell and differentiated C_2C_{12} cell. The black arrows point towards buddings ascribable to ERES. Scale bar: 500 nm. (B) Transmission EM (TEM) images of the perinuclear region of control and knockdown C_2C_{12} cells. GM130 and p115 depletion induces the formation of disordered, partially unstacked GC structures (GC) with few GC elements adjacent to the perinuclear ER. In parallel, the perinuclear ER from GM130- and p115-depleted cells presented less buds that are decorated with an electron-dense coat, ascribable to ERES (highlighted by black arrows) compared to Neg9- or GRASP65-knockdown cells. Scale bar: 1 µm. (C) Quantification (mean±s.d.) of ERES/µm for ER in the perinuclear rim, determined by measuring the length of the perinuclear ER underlying a GC structure and counting the number of electron-dense budding structures in the segment (*n*=26).

Interestingly, as shown in Fig. 6B, the analysis of thin sections obtained from siRNA-treated differentiated C_2C_{12} cells revealed that GM130 and p115 knockdown induced the formation of disordered, partially un-stacked GC structures with only a few GC elements adjacent to the perinuclear ER. Moreover, consistent with the data obtained by ERES immunofluorescence labelling (Fig. 5D), the number of ERES on the perinuclear ER in close proximity to GC elements was considerably reduced in GM130- and p115-knockdown cells, compared to GRASP65 knockdown or control cells (Fig. 6C).

GM130 and p115 knockdown inhibits M-cadherin transport to the plasma membrane and cell fusion

Although the expression levels of muscle differentiation markers α-actinin, JP2 and M-cadherin appeared unaffected in GM130 or p115 knockdown cells (Fig. 4D,E), cell morphological features were significantly altered compared to GRASP65 knockdown or control cells (Fig. 7A,B). At 48 h after induction of differentiation, GM130- or p115-knockdown cells showed a less-elongated morphology, were mainly mono-nucleated and showed a reduced fusion index compared to control cells (Fig. 7B). In addition while M-cadherin strongly accumulated at the plasma membrane in control cells, GM130 or p115 knockdown drastically inhibited the plasma membrane transport of this muscle-specific protein involved in myoblast fusion (Fig. 7C). In differentiating C_2C_{12} cells transfected with Neg9 or GRASP6-targeting siRNA, the M-cadherin-specific fluorescence intensity line plots showed two peaks, one close to the nuclear periphery (the nuclear envelope) and one at the cell periphery (the plasma membrane), with the plasma membrane peak exceeding the nuclear envelope one by almost factor of 2, consistent with an efficient ER-to-plasma membrane transport of M-cadherin (Fig. 7A, white arrowheads, see also line scans). In contrast, in cells treated with siRNAs targeting GM130 or p115, the plasma membrane-associated peak was drastically reduced or could not even be detected, and only the nuclear envelope-associated peak presented high fluorescence levels (Fig. 7A, white arrowheads, see also line scans). These data suggest that transport of M-cadherin from the ER to the plasma membrane in differentiating cells is strongly inhibited, with an accumulation of the marker in the nuclear envelope, thus indicating that ER exit of M-cadherin is most likely inhibited upon GM130 or p115 knockdown, and suggesting that these two proteins can affect the fusion capability by interfering with M-cadherin localisation at the sarcolemma.

Parallel experiments showed a significant reduction of the transport of the transport marker VSVG to the plasma membrane upon GM130 or p115 knockdown (Fig. 7D). Together with the observation that in undifferentiated cells GM130 or p115 knockdown had little to no effect on VSVG plasma membrane transport (Fig. 4B), this result suggests that while these two proteins may not be essential for transport of VSVG to the plasma membrane in undifferentiated C_2C_{12} cells, they become crucial for the formation of the ERES–GC units to facilitate transport during SKM differentiation. Indeed, when cells are differentiating, they need to sustain a more-intense and/or specialised trafficking of molecules responsible for further cell differentiation, such as M-cadherin.

DISCUSSION

The present work has been aimed at a better understanding of the importance and the mechanisms underlying the reorganisation of ERES and GC during SKM differentiation.

Our data suggest that during SKM differentiation, ERES and GC associate as dynamic units, which form the typical peripheral GC–ERES elements previously described (Lu et al., 2001).

Journal of Cell Science (2019) 132, jcs222083. doi:10.1242/jcs.222083

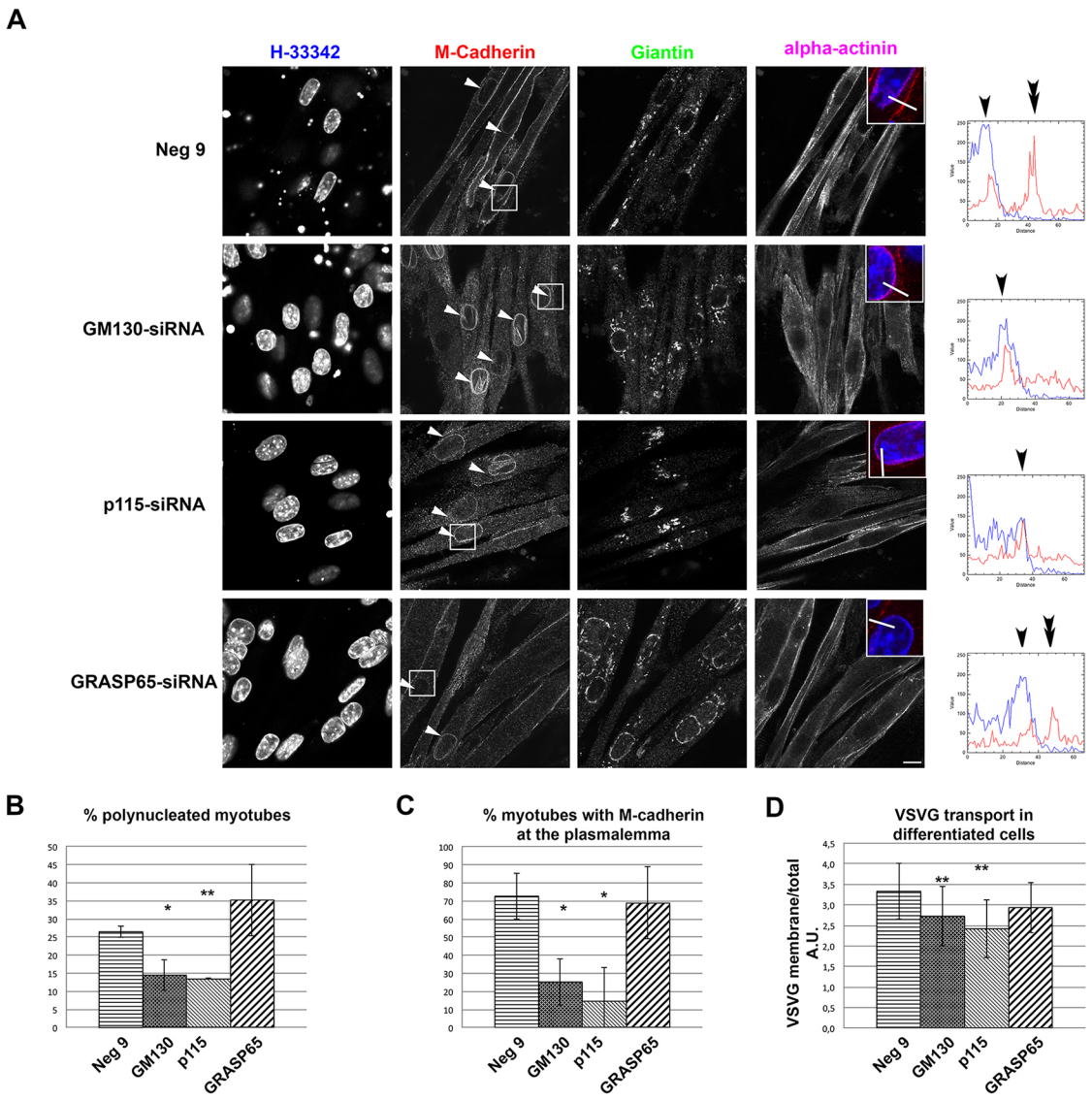

Fig. 7. Analysis of the effects of GM130 and p115 proteins knockdown on M-cadherin organisation. (A) Cells subjected to siRNA knockdown were stained with anti-M-cadherin and anti-giantin antibodies, and anti-α-actinin antibody, as marker for differentiating SKM cells; nuclei are stained with Hoechst 33342. In control cells (Neg9), the M-cadherin signal is mainly localised at the cell membranes and, to a lesser extent, at the perinuclear region at the level of giantin signal (see white arrowheads). GM130 and p115 knockdown cause a significant reduction of the M-cadherin signal at the plasmalemma. Interestingly, these cells show a strong M-cadherin signal at the perinuclear region (white arrowheads). The magnified insets capture an image area with both the perinuclear region and the plasma membrane. Line scans have been drawn passing from the nucleus to the plasma membrane, for the Neg9- and GRASP65-treated cells, the M-cadherin fluorescence intensity line shows two peaks close to the nuclear periphery (black arrowheads) and at the plasma membrane (black double arrowheads), with the plasma membrane peak exceeding the nuclear envelope one by a factor of almost 2, while GM130- and p115-treated cells prevalently show a fluorescence peak nearby at the nucleus periphery. Scale bar: 10 µm. (B) Fusion index of differentiating myotubes. (C) The percentage of myotubes with M-cadherin staining at the plasma membrane. (D) The efficiency of VSVG transport to the membrane. Data reported are the mean±s.d. of three independent experiments; **P*<0.05, ***P*<0.01.

Time-lapse analyses of this reorganisation indicates that the respective GC elements form from pre-existing Golgi membranes, rather than being synthesised *de novo*. Whether ERES are forming mainly around GC elements, or whether the GC attracts an increasing number of ERES while moving through the cell body could not be resolved by our time-lapse analyses and remains to be elucidated.

The organisation of GC–ERES that we have described here is comparable to the one previously described in plants (Brandizzi and Barlowe, 2013; Brandizzi and Barlowe, 2014; daSilva et al., 2004), and *Drosophila melanogaster* S2 cells (Kondylis and Rabouille, 2009), where the GC and ERES form intimately associated units.

Our data here show that knockdown of GM130 and p115 inhibits the formation of these units in differentiating cells and inhibits cell fusion by reducing M-cadherin transport to the plasma membrane. Interestingly, in undifferentiated cells, the depletion of GM130, p115 and GRASP65 has no apparent effect on the morphology of the GC and no major functional effects on the ER-to-plasma membrane transport efficiency of the established transport marker VSVG, but reduces the number of ERES surrounding it by a factor of almost 2. Also, GM130- or p115-knockdown cells are able to start their differentiation programme by expressing early differentiation markers such as α-actinin, JP2 and M-cadherin, similar to control cells. Therefore, we conclude that the p115 or

Journal of Cell Science (2019) 132, jcs222083. doi:10.1242/jcs.222083

GM130 knockdown-related reduction of ERES or any possible alterations of ERES–Golgi communication, which we have not so far observed in our experiments, at the undifferentiated stage, do not alter the ability of the cells to enter the early SKM differentiation programme. However, when differentiation progresses, and the ERES and GC undergo a more profound reorganisation in control or GRASP65-knockdown cells, we do see that GM130 and p115 depletion impairs this reorganisation, that VSVG transport to the membrane significantly reduced and that M-cadherin transport to the plasma membrane is strongly inhibited at the ER level. This suggests that the reorganisation of ERES and GC into stably associated units plays a crucial role for the efficient transport of differentiation-specific cargo during terminal SKM differentiation. Consistent with this is the fact that the degree of transport inhibition of VSVG appears rather marginal compared to the inhibition of M-cadherin, which may be explained by the possibility that the viral protein VSVG, in contrast to endogenous M-cadherin, may also be able to use p115- and GM130-independent routes to leave the ER.

Our results showing that GM130, p115 and GRASP65 depletion reduce the number of ERES in undifferentiated cells, while in differentiated cells GRASP65-knockdown cells behave like control cells may appear contradictory. However, in our view these data reinforce the muscle differentiation-specific role(s) of GM130 and p115. Moreover, these data underline the importance of the reorganisation of the early secretory pathway for the SKM differentiation process. Organising GC and ERES in units throughout the cell body may have the advantage that transport carriers, forming at ERES, do not need to travel long distances along microtubules to reach their target, as previously shown in fibroblast-like cells (Scales et al., 1997). Myoblasts are characterised by a packed cytoplasm where movement of larger long-range carriers (VTCs; Scales et al., 1997) may be difficult or even impossible, and thus the ERES–GC units can guarantee efficient ER-to-GC transport. Interference with their function, as found upon knockdown of GM130 or p115, thus results in transport inhibition to the plasma membrane and therefore lack of essential factors at that location, which are required for cell fusion. We can speculate that this could reflect the need for either an increased efficiency of transport in general or for specific transport routes that need to be activated during the differentiation process.

How GM130 or p115 are involved in the reorganisation of GC and ERES is still an open question. The two proteins could participate in tethering mechanisms linking ERES with GC structures through the interaction of GM130 and p115 (Seemann et al., 2000). Alternatively, GC structures could generate a signalling microenvironment that leads to ERES formation in the proximity of GC structures, a process that might be regulated by GM130 and/or p115. In fact, data obtained by BFA treatment and siRNA-mediated depletion suggest that, in differentiating SKM cells, ERES preferentially organise around a GC remnant structure associated with GM130. This is in agreement with earlier data (Ronchi et al., 2014) proposing that GC can induce ERES biogenesis. Our data therefore support the hypothesis that the GC exerts a hub function in the regulation of transport via the modulation of vesicle distribution, fusion, ERES assembly and localisation (Luini and Parashuraman, 2016; Ronchi et al., 2014) and thus confer, to the GC, a central role in the organisation of ERES in a physiological environment such as SKM differentiating cells.

Studies on skeletal muscles obtained from dystrophic models showed that the sorting and trafficking of correctly processed proteins and lipids from the GC to the sarcolemma are required for the maintenance of sarcolemmal integrity during the repeated contraction-relaxation cycles, preventing injury (Percival and Froehner, 2007). Until now, it has not been directly determined whether and how changes to GC morphology could interfere with SKM function.

Our data showing that GM130 and p115 knockdown can interfere with M-cadherin transport and affecting the index of fusion, demonstrate a functional link between GC–ERES organisation and the early phases of SKM differentiation and allocates to GM130 and p115 a central role in this process. Different from the observation that the reorganisation of GC and ERES can occur despite the lack of myoblast fusion (Ralston, 1993), our data suggest that GC and ERES organisation have an essential role in this process by participating in the targeting of M-cadherin to the plasma membrane. In turn, the lack of M-cadherin at the plasma membrane could itself trigger a cascade of effects on SKM differentiation. In fact, M-cadherin targeting at cell–cell contacts during myoblast fusion has been shown to be responsible of the Rac1 GTPase cascade activation (Charrasse et al., 2007), providing to M-cadherin a role in the activation of the promyogenic cascade.

Interestingly, recent work (Shamseldin et al., 2016) has attributed an important role to GM130 during muscle development by finding and characterising a homozygous frame-shift mutation in this protein. The mutation was found in a patient with a neuromuscular disorder who presented with developmental delay, seizures, progressive microcephaly and muscular dystrophy. The authors showed that the truncated protein is either not produced or is very unstable, suggesting that this is close to a null mutation where GM130 functions are largely lost. These results are consistent with our finding that GM130 and p115 are essential for the regulation of SKM differentiation in C_2C_{12} cells.

In summary, our work shows for the first time that a coordinated reorganisation of the GC and ERES is required for the correct transport of M-cadherin during SKM differentiation, and that loss of the integrity of their association leads to defective differentiation. GM130 and p115 play a fundamental role in the formation and maintenance of GC–ERES units, therefore ensuring the correct delivery to the plasma membrane of proteins that are fundamental for SKM differentiation, such as M-cadherin.

MATERIALS AND METHODS

Plasmids and siRNA

The Golgi–CFP plasmid encoding for 81 amino acids of the precursor to the human β-1,4-galactosyltransferase (Clontech Laboratories), and Sec23a–EYFP plasmid (Forster et al., 2006) were used in live imaging experiments. ts-O45-G–CFP was obtained from Kai Simons (MPI-CBG, Dresden, Germany). The following Silencer Select siRNAs (Ambion, Thermo Fisher) were used: GM130 (s97432), p115 (s80014), GRASP65 (s92890), and Silencer Select Negative Control 9 siRNA (Neg9; s444246).

Antibodies

The following antibodies were used in immunofluorescence (IF) and western blotting (WB) according the manufacturer's instructions at the dilutions indicated. Primary antibodies were: mouse anti-α-actinin (clone EA-53, Sigma-Aldrich; IF, 1:1000; WB, 1:1000), mouse anti-PDI (clone 1D3, Enzo Life Sciences; IF, 1:200), mouse anti-M-cadherin (clone 12-G4, Merck-Millipore; IF, 1:200; WB, 1:500), goat anti-JP2 (Y-15, Santa Cruz Biotechnology; WB, 1:1000), mouse anti-GM130 (clone 35GM130, BD Biosciences; IF, 1:500), rabbit anti-GM130 (Ab52649, Abcam; WB, 1:500), mouse anti-giantin (clone G1/33, Enzo Life Sciences; IF, 1:1000), rabbit anti-giantin (Ab24586, Abcam, IF, 1:2000), rabbit anti-GRASP65 (Ab30315, Abcam; IF, 1:200; WB, 1:500), rabbit anti-p115 (13509-1-AP, Proteintech; IF, 1:200; WB, 1:500), rabbit anti-Sec13 (1:100 for IF; Verissimo et al., 2015), rabbit-anti Lamin B1 (Ab16048, Abcam; WB, 1:2000), mouse anti p62-FITC conjugated (clone 53, BD Biosciences; IF, 1:100), rabbit anti-EAGE (1:2000 for IF; Pepperkok et al., 1993), and mouse anti-VSVG (1:100 for IF; Kreis, 1986). The secondary antibodies used in

immunofluorescence were purchased from Thermo Fisher Scientific; horseradish peroxidase (HRP)-conjugated secondary antibodies for western blot analysis were purchased from Sigma-Aldrich.

Cell culture and transfection

The mouse myogenic cell line C_2C_{12} was obtained from the American Type Culture Collection (http://www.lgcstandards-atcc.org/). Cells were maintained in DMEM high-glucose culture medium (Gibco) supplemented with 10% (v/v) heat inactivated fetal calf serum (Gibco), 2 mM glutamine (Gibco), 1 mM pyruvate (Gibco), according to ATCC guidelines. For plasmid transfection, 100,000 cells were subcultured on gelatin-coated 35 mm glass bottom microwell dishes (MatTek), and, the following day, transfected with Lipofectamine Plus reagent (LifeTechnologies) and switched into differentiation medium (high-glucose DMEM containing 2% horse serum). Live-cell imaging was performed in phenol-free differentiation medium. For siRNA experiments, cells were plated on 35 mm dishes or eight-well Lab-Teks (Nunc) gelatin-coated plates (100,000 and 8000 cells per well, respectively) and transfected with siRNAs with RNAiMax reagent (LifeTechnologies) according to the manufacturer's instructions. Cells were allowed to grow in culture medium and switched to differentiation medium after 48 h. Samples were processed for western blot, immunofluorescence labelling or live imaging experiments at selected time points as indicated in the results section. The efficiency of knockdown of GM130, p115 and GRASP65, was routinely verified by western blot (Fig. 4C) and immunostaining.

VSVG–CFP transport assay

Cells transfected with siRNA were infected with a VSVG–CFP-encoding adenovirus, ts-O45-G–CFP, for 1 h at 37°C and incubated for 16 h at 39°C (Keller et al., 2001). To release the temperature-dependent transport block, cells were incubated at 32°C for 45 min and then fixed. Fixed cells were stained with an anti-VSVG antibody and imagined with a multi-position wide-field microscope Scan R (Olympus).

Immunofluorescence staining

Cells were fixed with 3% paraformaldehyde, in PBS (137 mM NaCl, 2.7 mM KCl, 4.3 mM Na_2HPO_4, 1.4 mM KH_2PO_4) for 20 min at room temperature. After extensive washing, cells were permeabilised with 0.5% Triton X-100 in PBS, washed, and incubated for 60 min in PBS with 5% goat serum in order to reduce unspecific binding. Cells were then incubated with primary antibody, extensively washed and then incubated with secondary antibodies following the manufacturer's instructions. Hoechst 33342 (Sigma-Aldrich) was added to the secondary antibody solution to stain nuclei.

EM analysis

Cells growing on MatTek dishes were fixed by addition of 2.5% glutaraldehyde (GA; Electron Microscopy Sciences) in 0.1 M cacodylate buffer. All the subsequent EM processing steps (OSO_4, Uranyl Acetate, dehydration, Epon embedding) were performed using a PELCO Biowave Pro microwave processor (Ted Pella) as described in Schieber et al., 2010. The cells were flat-embedded. After polymerisation of the resin at 60°C for 48 h, the coverslips were removed, therefore exposing the cell monolayers at the block surface. The blocks were then sectioned with a Leica UC7 microtome. 70 nm or 300 nm thick sections were collected on Formvar-coated slot grids and imaged with a Philips Biotwin CM120 (for 2D imaging of thin sections) or a FEI Tecnai F30 (for tomography) electron microscope. For the image shown in Fig. 6A, tilt series were acquired and then the tomograms were reconstructed and segmented with the IMOD software package (Kremer et al., 1996). The quantification of ERES from EM micrographs reported in Fig. S2C was performed by counting the number of ERES and normalising for the length of the ER sheets within ∼1 µm of the surface of the nearest GC. Data are reported as number of ERES per µm ER in proximity to the GC structure. The quantification of ERES per µm for ER in the perinuclear region reported in Fig. 6 was determined by measuring the length of the perinuclear ER underlying a GC structure and counting the number of electron-dense budding structures in the segment.

Cell imaging and image analysis

Live imaging of differentiating C_2C_{12} cells was carried out with a multi-position time-lapse spinning disc confocal microscope VOX (Perkin Elmer) equipped with an incubation chamber at 37°C with 5% CO_2. Living cells were imaged in high-glucose DMEM without Phenol Red containing 2% horse serum. Videos obtained with the VOX microscope were processed and analysed with Volocity software.

3D images were processed with Volocity software to calculate the proximity of ERES to the GC (Fig. S1). GC and ERES fluorescence signals were segmented, and the ratio between ERES fluorescence in GC and the total ERES fluorescence was plotted along the time in the graph for several cells.

Specimens obtained by immunofluorescence staining, were imaged with the VOX spinning disc confocal microscope (Perkin Elmer), the LSM510-Meta (Zeiss) and the SP5 laser scanning confocal microscopes (Leica Microsystems) or with the multi-position time-lapse wide field microscope Scan R (Olympus) depending on the experiment. Colocalisation analyses reported in Fig. 1 were performed on images obtained with the VOX spinning disc confocal microscope (Perkin Elmer), deconvolved with Huygens software (Scientific Volume Imaging) and further analysed for colocalisation with the Volocity software.

Image analyses for the VSVG assay were manually performed with Fiji software by calculating the ratio between fluorescence at the membrane and total VSVG fluorescence.

Immunofluorescence determination of ERES colocalising with the GC in undifferentiated cells was performed with Volocity software. ERES and GC signals were segmented and the relative number of ERES superimposing with the GC was calculated by dividing the ERES colocalising with GC by the GC surface area.

ERES localisation at the perinuclear region of differentiated myotubes was calculated manually with Fiji software by drawing a ring around each nucleus at the level of p62 signal and an outer ring, adjacent to the first, that were both 4 pixels wide (resolution of the images 8.4 pixels/µm). The mean fluorescence was measured for each ring in the Sec13 channel. Results are expressed as ratio of the florescence signal between the inner and the outer ring (see Fig. S4B).

Western blots

For western blot analysis, C_2C_{12} cells were transfected in 35 mm Petri dishes, after 48 h differentiation were washed in PBS and, whole-cell extracts were prepared by directly adding 200 µl of 2× Laemmli buffer to the dishes, and lysates were scraped, collected in tubes and Benzonase (Merck Millipore) and $MgCl_2$ were added for 10 min at room temperature. Heat-denatured samples were run on NuPage Bis-Tris Gels (4–12%, Thermo Fisher Scientific) and transferred onto pre-activated PVDF membranes. The membranes were saturated in PBS containing 0.2% Tween 80 (PBS-T) and 5% dry milk, incubated with the primary antibodies, extensively washed with PBS-T, incubated with the appropriated HRP-conjugated antibodies, washed extensively and revealed with a Pierce western blotting detection kit (Thermo Fisher Scientific). Fiji was utilised to quantify the intensities of immunoreactive bands from three independent experiments; sample loading was normalised to anti-Lamin B1 immunoreactive bands.

Statistical analyses

Student's two tailed *t*-test analyses were performed using GraphPad Prism version 7.00 for Windows (GraphPad) and Microsoft Excel. Data are expressed as means±s.d.

Acknowledgements

Support of the EMCF and ALMF core facilities at EMBL-Heidelberg is acknowledged. We thank Fatima Verissimo and Nurlanbek Duishuev for helpful discussions, Christian Tischer and Yury Belyaev for invaluable help in image analysis. The authors also thank the members of the Rainer Pepperkok team for discussion and support.

Competing interests

The authors declare no competing or financial interests.

Author contributions

Conceptualization: E.G., R.P.; Methodology: E.G., P.R.; Investigation: E.G.; Resources: R.P.; Data curation: E.G., P.R.; Writing - original draft: E.G., R.P.; Writing - review & editing: E.G., R.P., P.R.; Funding acquisition: E.G., R.P.

Funding
This work was supported by the European Molecular Biology Laboratory (EMBL); E.G. was funded by a Marie Curie IEF fellowship from the Seventh Framework Programme (grant 326691-TRAFFIC IN SKM) and iNEXT project 2435, funded by the Horizon 2020 programme of the European Commission (grant number 653706).

Supplementary information
Supplementary information available online at
http://jcs.biologists.org/lookup/doi/10.1242/jcs.222083.supplemental

References

Barr, F. A., Puype, M., Vandekerckhove, J. and Warren, G. (1997). GRASP65, a protein involved in the stacking of Golgi cisternae. *Cell* **91**, 253-262.
Barr, F. A., Nakamura, N. and Warren, G. (1998). Mapping the interaction between GRASP65 and GM130, components of a protein complex involved in the stacking of Golgi cisternae. *EMBO J.* **17**, 3258-3268.
Bexiga, M. G. and Simpson, J. C. (2013). Human diseases associated with form and function of the Golgi complex. *Int. J. Mol. Sci.* **14**, 18670-18681.
Brandizzi, F. and Barlowe, C. (2013). Organization of the ER-Golgi interface for membrane traffic control. *Nat. Rev. Mol. Cell Biol.* **14**, 382-392.
Brandizzi, F. and Barlowe, C. (2014). ER-Golgi transport: authors' response. *Nat. Rev. Mol. Cell Biol.* **15**, 1.
Braun, T. and Gautel, M. (2011). Transcriptional mechanisms regulating skeletal muscle differentiation, growth and homeostasis. *Nat. Rev. Mol. Cell Biol.* **12**, 349-361.
Buckingham, M. and Rigby, P. W. J. (2014). Gene regulatory networks and transcriptional mechanisms that control myogenesis. *Dev. Cell* **28**, 225-238.
Charrasse, S., Comunale, F., Fortier, M., Portales-Casamar, E., Debant, A. and Gauthier-Rouviere, C. (2007). M-cadherin activates Rac1 GTPase through the Rho-GEF trio during myoblast fusion. *Mol. Biol. Cell* **18**, 1734-1743.
daSilva, L. L., Snapp, E. L., Denecke, J., Lippincott-Schwartz, J., Hawes, C. and Brandizzi, F. (2004). Endoplasmic reticulum export sites and Golgi bodies behave as single mobile secretory units in plant cells. *Plant Cell* **16**, 1753-1771.
Doberstein, S. K., Fetter, R. D., Mehta, A. Y. and Goodman, C. S. (1997). Genetic analysis of myoblast fusion: blown fuse is required for progression beyond the prefusion complex. *J. Cell Biol.* **136**, 1249-1261.
Donalies, M., Cramer, M., Ringwald, M. and Starzinski-Powitz, A. (1991). Expression of M-cadherin, a member of the cadherin multigene family, correlates with differentiation of skeletal muscle cells. *Proc. Natl. Acad. Sci. USA* **88**, 8024-8028.
Forster, R., Weiss, M., Zimmermann, T., Reynaud, E. G., Verissimo, F., Stephens, D. J. and Pepperkok, R. (2006). Secretory cargo regulates the turnover of COPII subunits at single ER exit sites. *Curr. Biol.* **16**, 173-179.
Franzini-Armstrong, C. (2004). The membrane systems of muscle cells. In *Myology* (ed. A. Engel and C. Franzini-Armstrong), pp. 232-256. New York: Mc Graw-Hill.
Glick, B. S. (2014). Integrated self-organization of transitional ER and early Golgi compartments. *BioEssays* **36**, 129-133.
Kaisto, T. and Metsikko, K. (2003). Distribution of the endoplasmic reticulum and its relationship with the sarcoplasmic reticulum in skeletal myofibers. *Exp. Cell Res.* **289**, 47-57.
Keller, P., Toomre, D., Díaz, E., White, J. and Simons, K. (2001). Multicolour imaging of post-Golgi sorting and trafficking in live cells. *Nat. Cell Biol.* **3**, 140-149.
Kondylis, V. and Rabouille, C. (2009). The Golgi apparatus: lessons from Drosophila. *FEBS Lett.* **583**, 3827-3838.
Kreis, T. E. (1986). Microinjected antibodies against the cytoplasmic domain of vesicular stomatitis virus glycoprotein block its transport to the cell surface. *EMBO J.* **5**, 931-941.
Kremer, J. R., Mastronarde, D. N. and McIntosh, J. R. (1996). Computer visualization of three-dimensional image data using IMOD. *J. Struct. Biol.* **116**, 71-76.
Lippincott-Schwartz, J., Yuan, L. C., Bonifacino, J. S. and Klausner, R. D. (1989). Rapid redistribution of Golgi proteins into the ER in cells treated with brefeldin A: evidence for membrane cycling from Golgi to ER. *Cell* **56**, 801-813.
Lu, Z., Joseph, D., Bugnard, E., Zaal, K. J. M. and Ralston, E. (2001). Golgi complex reorganization during muscle differentiation: visualization in living cells and mechanism. *Mol. Biol. Cell* **12**, 795-808.
Luini, A. and Parashuraman, S. (2016). Signaling at the Golgi: sensing and controlling the membrane fluxes. *Curr. Opin. Cell Biol.* **39**, 37-42.
Nakamura, N. (2010). Emerging new roles of GM130, a cis-Golgi matrix protein, in higher order cell functions. *J. Pharmacol. Sci.* **112**, 255-264.
Nakamura, N., Lowe, M., Levine, T. P., Rabouille, C. and Warren, G. (1997). The vesicle docking protein p115 binds GM130, a cis-Golgi matrix protein, in a mitotically regulated manner. *Cell* **89**, 445-455.
Pepperkok, R., Scheel, J., Horstmann, H., Hauri, H. P., Griffiths, G. and Kreis, T. E. (1993). Beta-COP is essential for biosynthetic membrane transport from the endoplasmic reticulum to the Golgi complex in vivo. *Cell* **74**, 71-82.
Percival, J. M. and Froehner, S. C. (2007). Golgi complex organization in skeletal muscle: a role for Golgi-mediated glycosylation in muscular dystrophies? *Traffic* **8**, 184-194.
Pouliot, Y., Gravel, M. and Holland, P. C. (1994). Developmental regulation of M-cadherin in the terminal differentiation of skeletal myoblasts. *Dev. Dyn.* **200**, 305-312.
Ralston, E. (1993). Changes in architecture of the Golgi complex and other subcellular organelles during myogenesis. *J. Cell Biol.* **120**, 399-409.
Ralston, E., Lu, Z. and Ploug, T. (1999). The organization of the Golgi complex and microtubules in skeletal muscle is fiber type-dependent. *J. Neurosci.* **19**, 10694-10705.
Ronchi, P., Tischer, C., Acehan, D. and Pepperkok, R. (2014). Positive feedback between Golgi membranes, microtubules and ER exit sites directs de novo biogenesis of the Golgi. *J. Cell Sci.* **127**, 4620-4633.
Rossi, D., Barone, V., Giacomello, E., Cusimano, V. and Sorrentino, V. (2008). The sarcoplasmic reticulum: an organized patchwork of specialized domains. *Traffic* **9**, 1044-1049.
Scales, S. J., Pepperkok, R. and Kreis, T. E. (1997). Visualization of ER-to-Golgi transport in living cells reveals a sequential mode of action for COPII and COPI. *Cell* **90**, 1137-1148.
Schieber, N. L., Nixon, S. J., Webb, R. I., Oorschot, V. M. and Parton, R. G. (2010). Modern approaches for ultrastructural analysis of the zebrafish embryo. *Methods Cell Biol.* **96**, 425-442.
Seemann, J., Jokitalo, E. J. and Warren, G. (2000). The role of the tethering proteins p115 and GM130 in transport through the Golgi apparatus in vivo. *Mol. Biol. Cell* **11**, 635-645.
Shamseldin, H. E., Bennett, A. H., Alfadhel, M., Gupta, V. and Alkuraya, F. S. (2016). GOLGA2, encoding a master regulator of golgi apparatus, is mutated in a patient with a neuromuscular disorder. *Hum. Genet.* **135**, 245-251.
Tangemo, C., Ronchi, P., Colombelli, J., Haselmann, U., Simpson, J. C., Antony, C., Stelzer, E. H. K., Pepperkok, R. and Reynaud, E. G. (2011). A novel laser nanosurgery approach supports de novo Golgi biogenesis in mammalian cells. *J. Cell Sci.* **124**, 978-987.
Tassin, A. M., Maro, B. and Bornens, M. (1985a). Fate of microtubule-organizing centers during myogenesis in vitro. *J. Cell Biol.* **100**, 35-46.
Tassin, A. M., Paintrand, M., Berger, E. G. and Bornens, M. (1985b). The Golgi apparatus remains associated with microtubule organizing centers during myogenesis. *J. Cell Biol.* **101**, 630-638.
Verissimo, F., Halavatyi, A., Pepperkok, R. and Weiss, M. (2015). A microtubule-independent role of p150glued in secretory cargo concentration at endoplasmic reticulum exit sites. *J. Cell Sci.* **128**, 4160-4170.
Volpe, P., Villa, A., Podini, P., Martini, A., Nori, A., Panzeri, M. C. and Meldolesi, J. (1992). The endoplasmic reticulum-sarcoplasmic reticulum connection: distribution of endoplasmic reticulum markers in the sarcoplasmic reticulum of skeletal muscle fibers. *Proc. Natl. Acad. Sci. USA* **89**, 6142-6146.
Zaal, K. J. M., Reid, E., Mousavi, K., Zhang, T., Mehta, A., Bugnard, E., Sartorelli, V. and Ralston, E. (2011). Who needs microtubules? Myogenic reorganization of MTOC, Golgi complex and ER exit sites persists despite lack of normal microtubule tracks. *PLoS ONE* **6**, e29057.
Zeschnigk, M., Kozian, D., Kuch, C., Schmoll, M. and Starzinski-Powitz, A. (1995). Involvement of M-cadherin in terminal differentiation of skeletal muscle cells. *J. Cell Sci.* **108**, 2973-2981.

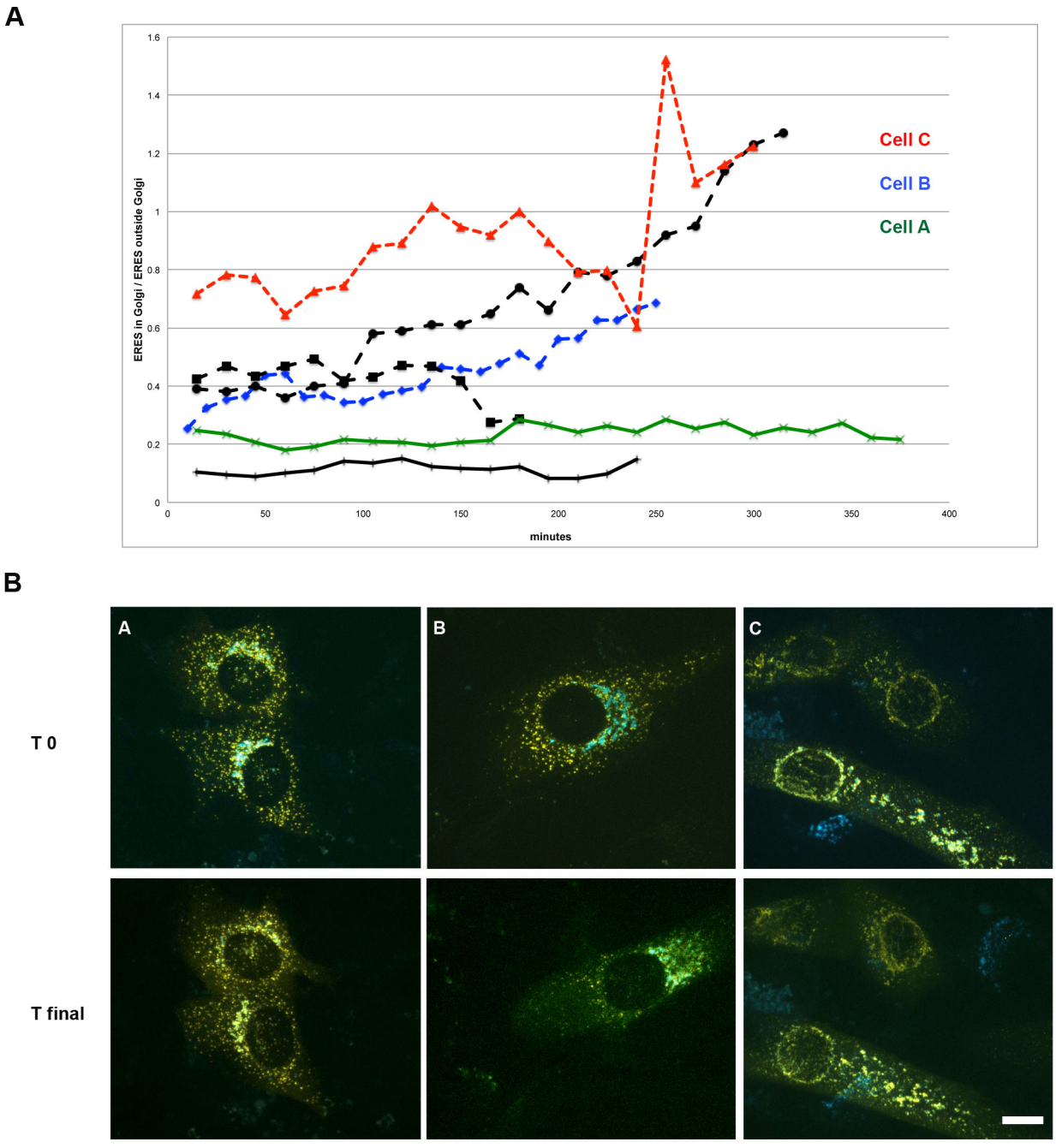

Figure S1. Live imaging of GC and ERES during C_2C_{12} differentiation. Cells were transfected with the plasmid pCFP-Golgi (in blue in the images) and the ERES protein Sec23a-YFP (in yellow) and imaged every 10-15 minutes for several hours in an incubation chamber by means of spinning-disk confocal microscope (Perkin Elmer). 3D images were processed with Volocity software. GC (CFP) and ERES (YFP) fluorescence signals were segmented and the ratio between ERES fluorescence in GC and the total ERES fluorescence was plotted along the time in the graph for several cells. The graph in panel A reports values for a total number of six cells, three representative cells are highlighted with different colours (Cell A in green, B in blue and C in red) and the correspondent still images at the beginning (T0) and end (Tfinal) of acquisition are reported in panel B. Cell A is a cell that does not undergo differentiation, the ratio ERES in Golgi/total ERES is low and does not change during time. Cell B is initially undifferentiated, the ratio ERES in Golgi/ total ERES at time 0 is low and gradually increases with the time. C represents a cell that at T0 is already in a differentiated state, the ratio is high and maintained along time. Bar 10 μm.

Journal of Cell Science • Supplementary information

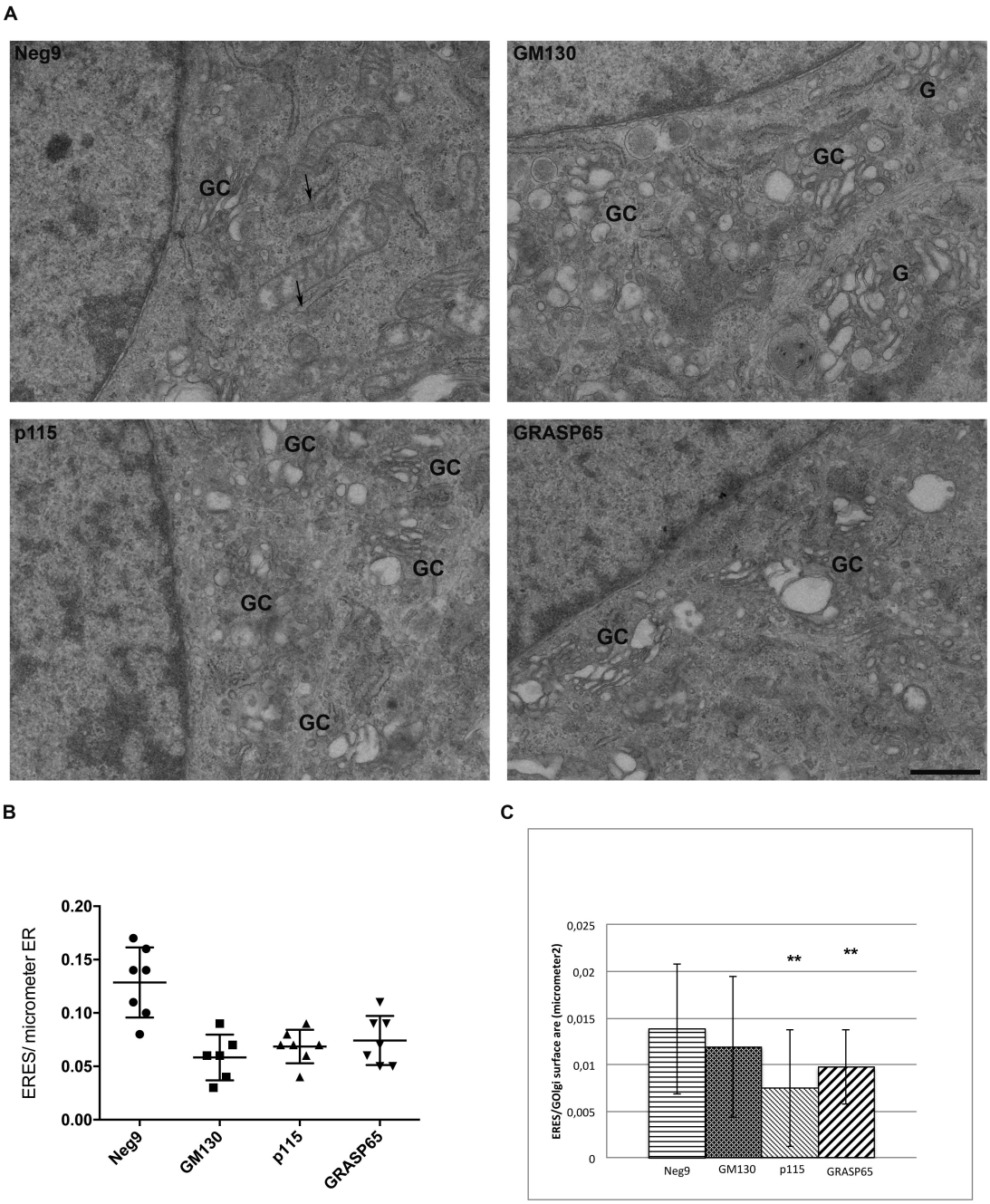

Figure S2. Analysis of GC and ERES reciprocal organisation in undifferentiated C2C12 cells upon GM130, p115, and GRASP65 knock-down. Cells were transfected with siRNAs, fixed after 48 hrs and then processed. Panel A reports TEM images of knock-down undifferentiated C_2C_{12} cells focusing on several GC elements. Arrows highlight ERES. Bar 1 µm. Graph in B reports the number of ERES per µm of ER, as quantified from TEM images (n=27). Graph in C reports the quantification of number of ERES colocalising with GC by immunofluorescence staining. Data reported are the mean of three independent experiments; **=$p<0.01$. Data are expressed as means ± SD.

Journal of Cell Science • Supplementary information

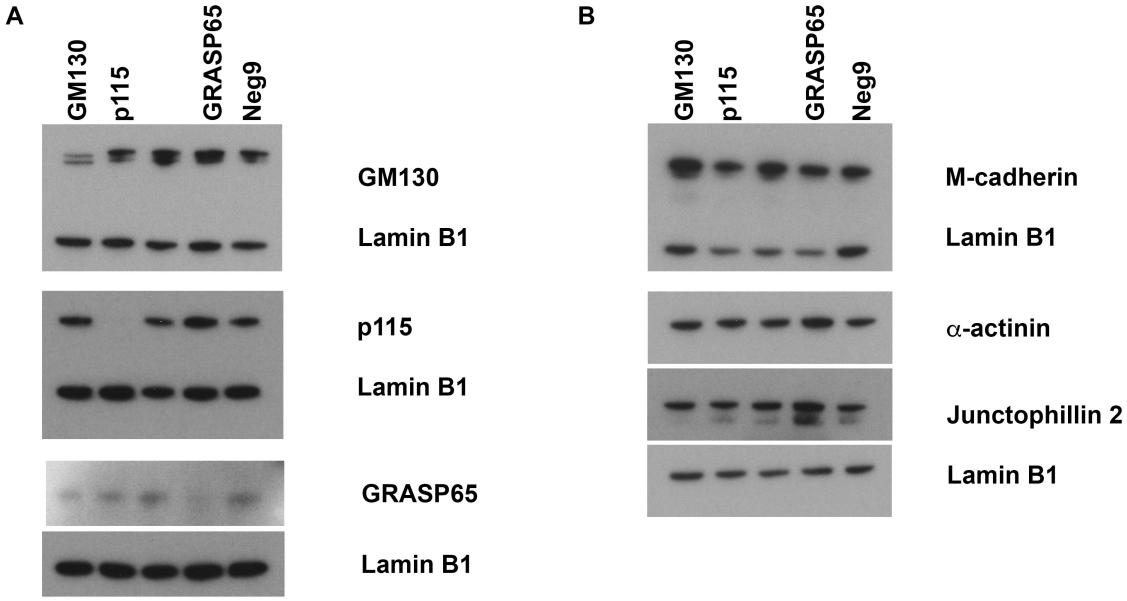

Figure S3. Protein expression analysis upon inhibition of GM130, p115, and GRASP65. Cells were transfected with siRNAs, after 48hrs induced to differentiation for 48hrs and then subjected to western blot analysis to detect the inhibition of GM130, p115 and the expression levels of SKM markers. Panel A reports protein expression levels upon inhibition of GM130, p115, and GRASP65 respectively. Panel B shows the expression levels of SKM markers as alpha-actinin, Junctophillin 2 (JP2) and M-cadherin. Protein load was normalised with Lamin B1.

Journal of Cell Science • Supplementary information

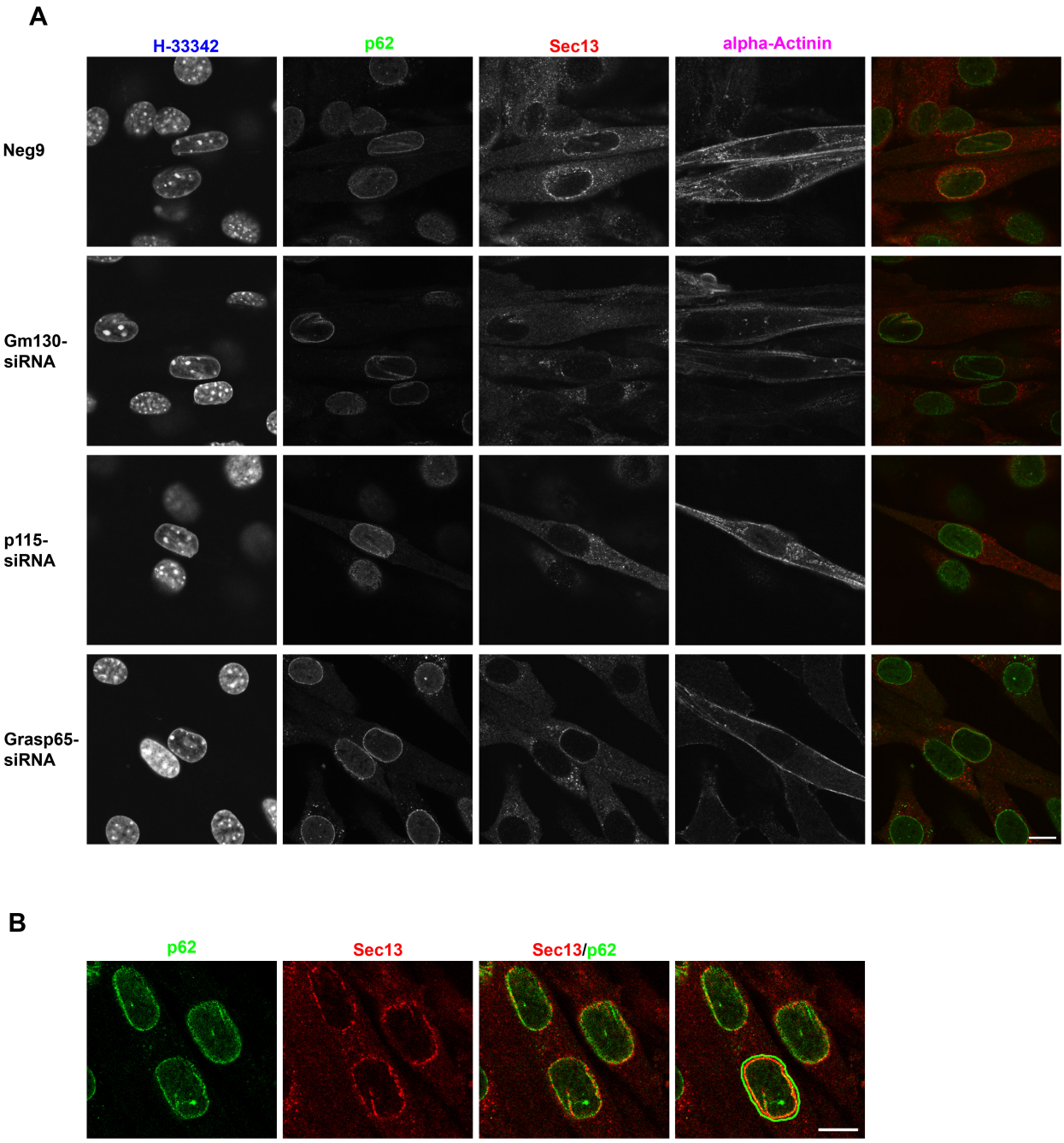

Figure S4. Analysis of the perinuclear localisation of ERES. Cells were transfected with siRNAs, after 48hrs induced to differentiation for further 48hrs, fixed and stained with anti p62-FITC, Sec13 and alpha-actinin antibodies. In Panel A representative pictures from control and knock-down cells are reported. In panel B an example of quantification is shown. A ring around each nucleus at the level of p62 signal (red line) and an outer ring (green line), adjacent to the first, both 4 pixels wide (resolution of the images 8.4 pixels/μm) were drawn as shown in the very left image. The mean fluorescence was measured for each ring in the Sec13 channel. Results are expressed as ratio between the inner and the outer ring fluorescence intensities. Bar 10 μm.

Journal of Cell Science • Supplementary information

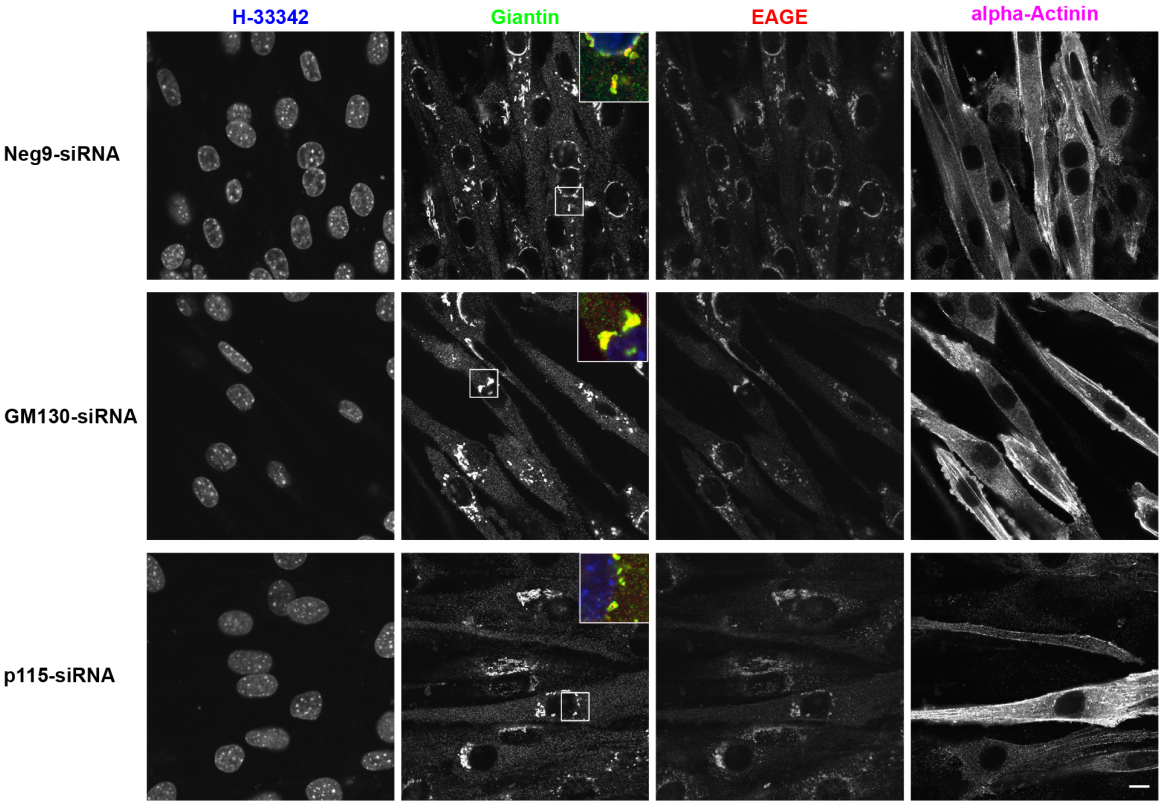

Figure S5: Effects of GM130 and p115 down regulation on COPI distribution in differentiating C_2C_{12}. Cells were transfected with the reported siRNAs, after 48hrs switched to differentiation medium and then fixed after 48hrs and stained with EAGE antibody, alpha-actinin marker was utilised to detect differentiating SKM cells, and Hoechst 33342 to stain nuclei. The zoom-in insets capture the perinuclear region to highlight giantin and COPI vesicles distribution at this site in different conditions. Bar 10 μm.

Journal of Cell Science • Supplementary information

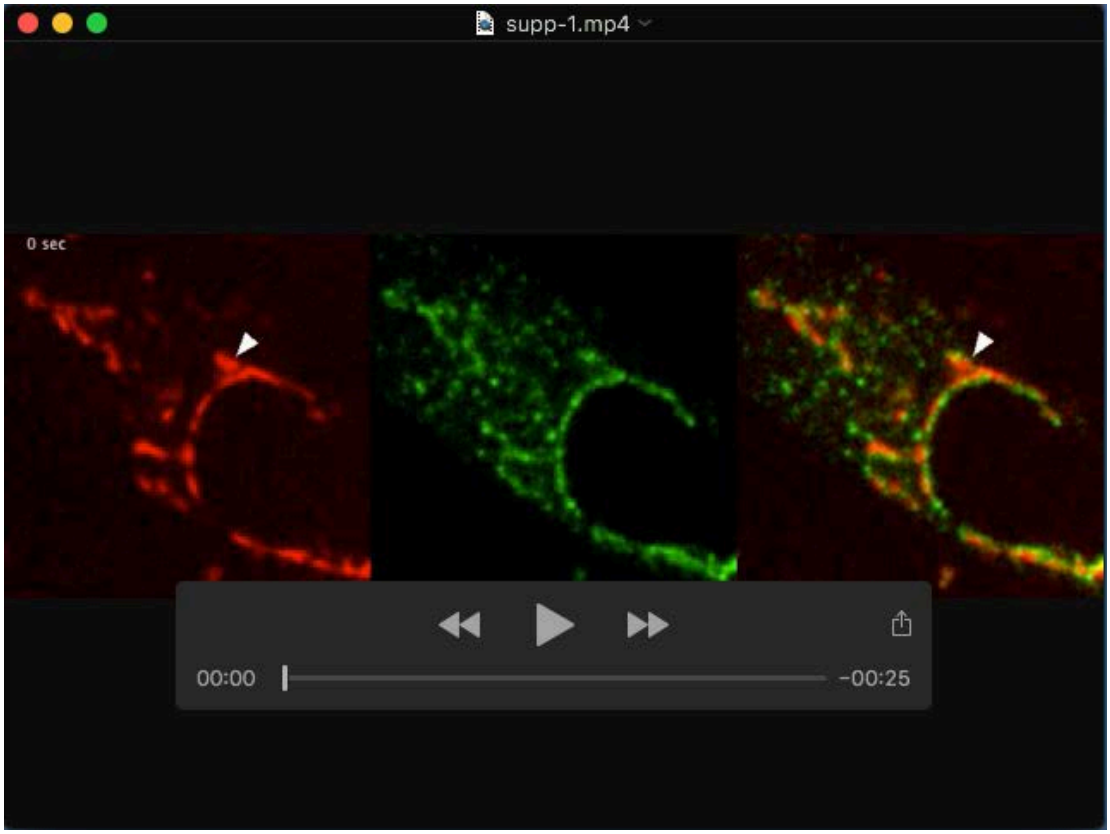

Movie 1: Time lapse imaging of a splitting event corresponding to Fig. 2A. C_2C_{12} were transfected with Golgi-CFP (red) and Sec23a-EYFP (green), induced to differentiate and imaged at the transition from phase 1 to 2 every 10-sec in the multi-position time-lapse spinning disk confocal microscope. Z-stacks covering the entire cell were acquired and sum projections are reported. The arrowheads and the arrows point towards 2 distinct splitting Golgi structures.

Journal of Cell Science • Supplementary information

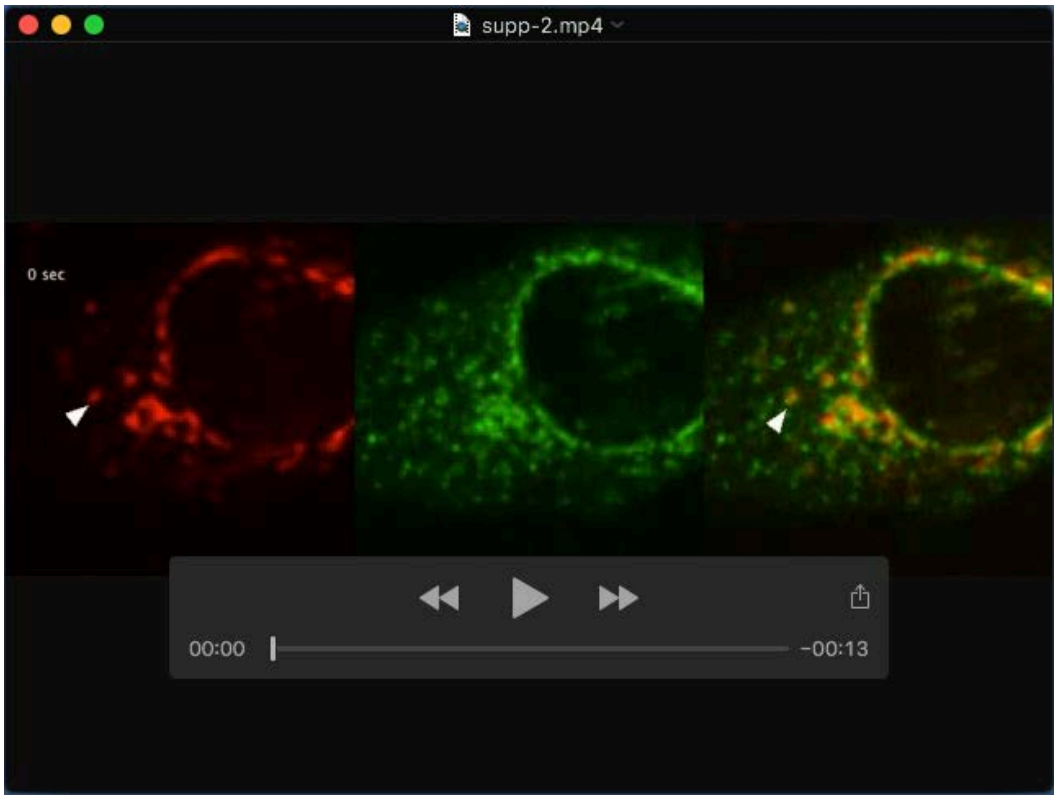

Movie 2: Time lapse imaging of a splitting event corresponding to Fig. 2B. C_2C_{12} cells were transfected with Golgi-CFP (red) and Sec23a-EYFP (green), induced to differentiate and imaged at the transition from phase 1 to 2 every 10-sec in the multi-position time-lapse spinning disk confocal microscope. Z-stacks covering the entire cell were acquired and sum projections are reported. The arrowheads point towards the splitting Golgi structures.

Journal of Cell Science • Supplementary information

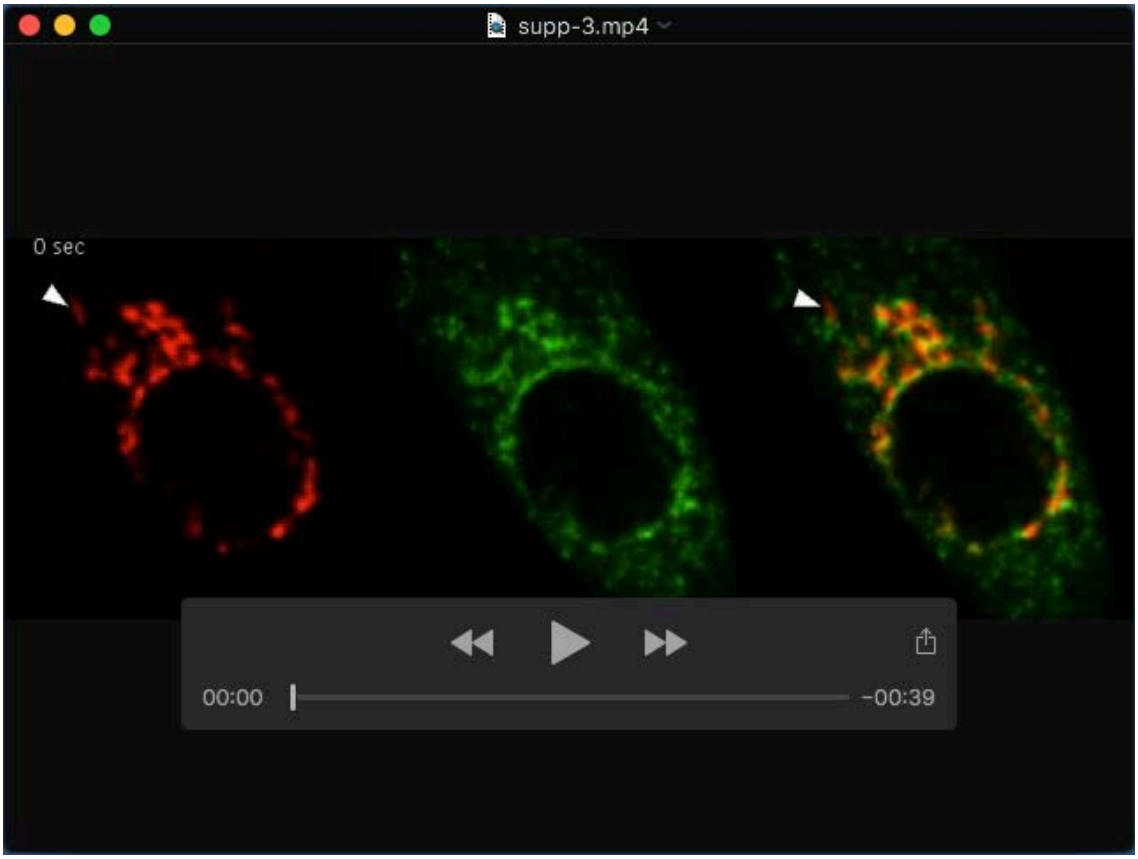

Movie 3: Time lapse imaging of merging event corresponding to Fig. 2C. C_2C_{12} cells were transfected with Golgi-CFP (red) and Sec23a-EYFP (green), induced to differentiate and imaged at the transition from phase 1 to 2 every 10-sec in the multi-position time-lapse spinning disk confocal microscope. Z-stacks covering the entire cell were acquired and sum projections are reported. The arrowhead towards the Golgi structure that undergo merging.

Journal of Cell Science • Supplementary information

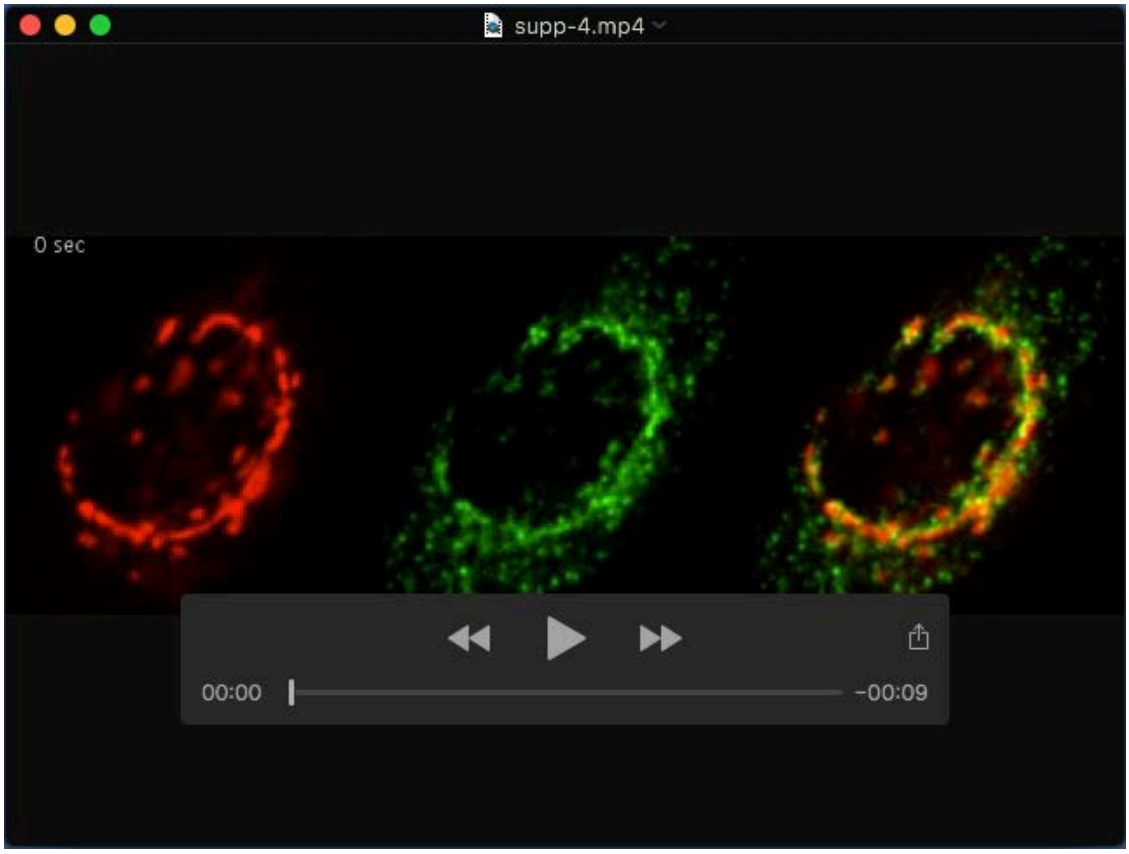

Movie 4. Time lapse imaging of a GC de novo biogenesis event corresponding to Fig. 2D. C_2C_{12} cells were transfected with Golgi-CFP (red) and Sec23a-EYFP (green), induced to differentiate and imaged at the transition from phase 1 to 2 every 10-sec in the multi-position time-lapse spinning disk confocal microscope. Z-stacks covering the entire cell were acquired and sum projections are reported. The arrowhead points towards the de novo formed Golgi structure.

Journal of Cell Science • Supplementary information

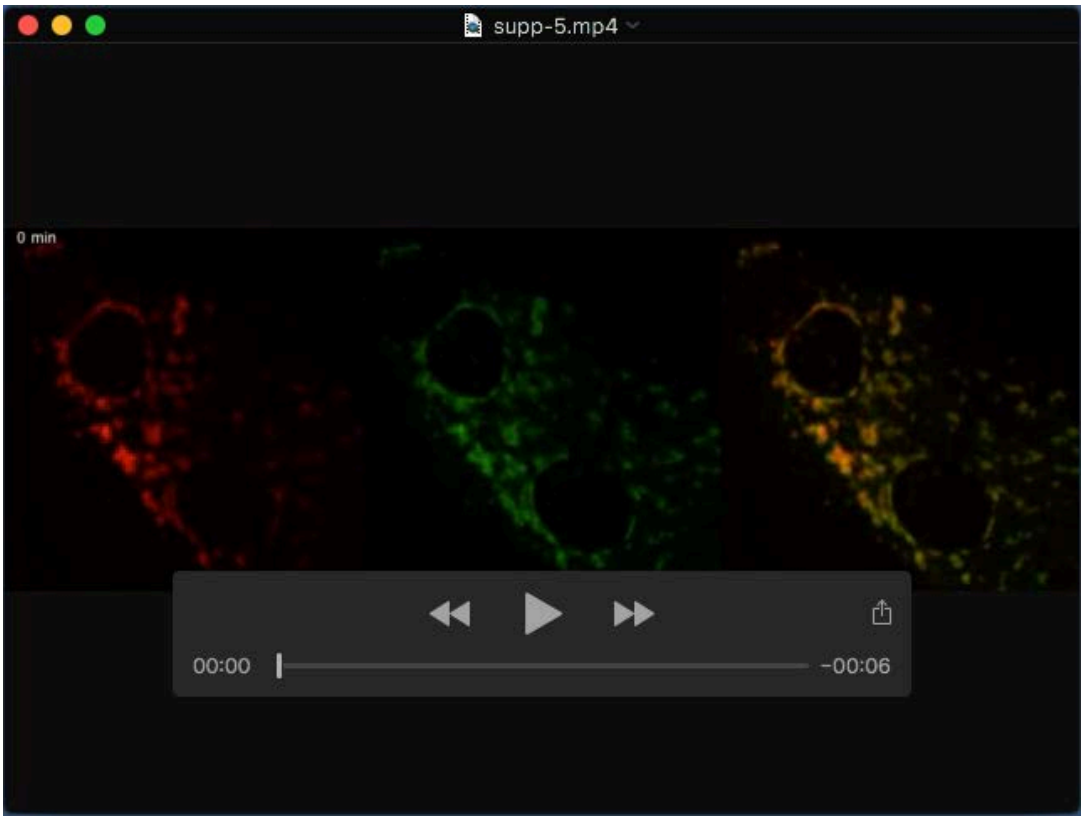

Movie 5. Time lapse imaging of BFA treatment in differentiating C_2C_{12} cells. C_2C_{12} cells were transfected with Golgi-CFP (red) and Sec23a-EYFP (green), induced to differentiation and treated with BFA. Cells imaged in the multi-position time-lapse spinning disk confocal microscope every 5 minutes. Z-stacks covering the entire cell were acquired and sum projections are reported.

Journal of Cell Science • Supplementary information